JGR Oceans

RESEARCH ARTICLE
10.1029/2025JC022808

Wave Projections for the Northeast Atlantic Using High Resolution Surrogate Winds

Ashly Kalayil Uthaman[1], Tomasz Dabrowski[2], Gerard D. McCarthy[1], and André Düsterhus[1,3]

[1]Irish Climate Analysis and Research Units (ICARUS), Department of Geography, Maynooth University, Maynooth, Ireland, [2]Ocean Science and Information Services Marine Institute Headquarters, Galway, Ireland, [3]National Centre for Climate Research (NCKF), Danish Meteorological Institute, Copenhagen, Denmark

Key Points:

- We developed a statistical-dynamical modeling framework to investigate wave climate in the North Atlantic
- An analog method is employed to generate high-resolution surrogates as wind boundary condition
- Wave height distribution shows seasonal trends, with future wave activity increasing in all seasons except autumn along Ireland's west coast

Correspondence to:

A. Kalayil Uthaman,
ashly.uthaman.2022@mumail.ie

Citation:

Kalayil Uthaman, A., Dabrowski, T., McCarthy, G. D., & Düsterhus, A. (2026). Wave projections for the Northeast Atlantic using high resolution surrogate winds. *Journal of Geophysical Research: Oceans*, *131*, e2025JC022808. https://doi.org/10.1029/2025JC022808

Received 28 AUG 2025
Accepted 17 APR 2026

Author Contributions:

Conceptualization: Ashly Kalayil Uthaman, Tomasz Dabrowski, Gerard D. McCarthy, André Düsterhus
Data curation: Ashly Kalayil Uthaman
Formal analysis: Ashly Kalayil Uthaman
Funding acquisition: André Düsterhus
Investigation: Ashly Kalayil Uthaman
Methodology: Ashly Kalayil Uthaman, Gerard D. McCarthy, André Düsterhus
Software: Ashly Kalayil Uthaman
Supervision: Gerard D. McCarthy, André Düsterhus
Validation: Ashly Kalayil Uthaman
Visualization: Ashly Kalayil Uthaman
Writing – original draft: Ashly Kalayil Uthaman
Writing – review & editing: Tomasz Dabrowski, Gerard D. McCarthy, André Düsterhus

Abstract Understanding projected changes in wave heights influenced by climate-driven factors, such as wind, sea ice, and sea level are essential for mitigating risks and ensuring sustainable use of marine and coastal resources, especially in a highly energetic wave region like the Northeast Atlantic (NEA). With a particular focus on Ireland, wave climate in the Northeast Atlantic region is investigated using wave models, WAM (WAve Model) and SWAN (Simulating WAves Nearshore). These are driven by high-resolution surrogate winds, incorporating sea ice and sea level as additional inputs. The surrogate wind data is created by an analog method using high-resolution wind data from the ECMWF atmospheric reanalysis data set to downscale data from the low-resolution Max-Planck Institute of Earth System Model (MPI-ESM-LR). This statistical approach provides computationally efficient and reliable wind inputs for wave modeling while capturing the temporal and spatial variability of present and future wind patterns. While the spatial distribution of significant wave height differences shows a north-south gradient, with an increase in the northern Northeast Atlantic and a decrease in the south, regional variability is evident. Seasonal analysis indicates pronounced increases in wave heights during winter and summer, with the largest decrease observed in autumn. This study demonstrates the efficiency of surrogate wind data for downscaling climate model outputs to support nearshore wave modeling. The findings underscore the importance of considering both regional and seasonal variability in wave climate assessments for proper coastal planning and adaptation strategies under changing climatic conditions.

Plain Language Summary Deeper insights on how waves behave are necessary for coastal communities, maritime activities and climate adaptation planning. Our study investigates wave height changes in the Northeast Atlantic (NEA) under the influence of climate-driven factors like wind, sea level, and sea ice. Accurate representation of wind fields is necessary for wave simulations. We address the limitation of coarse-resolution wind data from climate models for wave modeling, by implementing a method of generating high-resolution surrogates from observations. Surrogates are data behaving similar to original data set. For the current study we are using high-resolution, fifth-generation atmospheric reanalysis data as reference for generating surrogates for wind from a climate model. While overall wave heights are projected to increase in the northern NEA, it is important to carefully assess local variations. Instead of focusing only on extreme waves or specific events, our study looks at the full distribution of wave heights, offering valuable insights for better planning and adaptation strategies. For instance, some seasons may offer calmer and more stable conditions that are suitable for marine activities, while others see a rise in higher waves, depending on the location.

1. Introduction

Wind-generated surface waves are a significant renewable energy source (Farrok et al., 2024), and are important for many coastal processes, including erosion (Palermo et al., 2024; Scott et al., 2019) and the modulation of local trends of sea level (Dodet et al., 2019; Melet et al., 2018; Vousdoukas et al., 2017). This interaction between the wind and ocean surface wave is a fundamental component of the Earth system, with significant implications for climate modeling, coastal processes, and marine operations. These waves are not just surface phenomena but critical components of complex Earth system interactions, influencing everything from marine ecosystems to global climate patterns (Cavaleri et al., 2012). Understanding wave climate variability is particularly important in dynamic regions like the Northeast Atlantic (NEA), where the wave climate is significantly influenced by atmospheric patterns (Morales-Márquez et al., 2020), climate change, and seasonal patterns (Bitner-Gregersen et al., 2022; Markina et al., 2019; Morales-Márquez et al., 2020).

In addition to the broader climatic importance, ocean waves have significant societal implications for coastal regions. This is particularly relevant for Ireland, where the coastline is directly exposed to energetic North Atlantic wave conditions (Tiron et al., 2013). During storm events, high-energy waves can accelerate coastal erosion and contribute to overtopping of coastal defenses, with flooding further exacerbated by storm surges that pose a major risk to low-lying regions in terms of economic damage and casualties (Paranunzio et al., 2022). For example, during the exceptionally stormy winter of 2013–2014, a sequence of intense storms caused widespread coastal erosion and infrastructure damage exceeding €110 million along the south and west coasts of Ireland (Kandrot et al., 2016). More recently, during Storm Éowyn in January 2025, Galway city narrowly avoided severe flooding when a 2.6 m storm surge coincided with mid-tide conditions, highlighting the vulnerability of Irish coastlines (Madden et al., 2025). Furthermore, the economic implications of coastal flooding are expected to increase substantially under future sea level rise scenarios. De Bruin and Kyei (2024) estimates that without additional mitigation measures, the cost of a 0.56 m sea level rise is projected to reach approximately €3 billion by 2100 in Ireland, with potential GDP losses of up to 2.6% by 2030 in the absence of adaptation measures (De Bruin & Kyei, 2024). These costs are further compounded when extreme waves coincide with storm surges and elevated sea levels. Robust projections of future wave climates are therefore essential for coastal flood risk assessment and long-term adaptation planning.

The general concept of wave generation, propagation, and the transition from the deep ocean to the coastal environment involves downscaling the wave processes from oceanic to the regional and coastal scales. Various state-of-the-art wave models such as WAM (WAve Model; WAMdi Group, 1988), WW3 (WaveWatchIII; Tolman, 1989), and SWAN (Simulating WAves Nearshore; Booij et al., 1999) are implemented on nested grids to achieve fine-resolution wave simulations. For instance, Brown et al. (2010) and Pilar et al. (2008) effectively demonstrated that a North Atlantic (NA) domain, when used with a nested WAM model, is sufficient to capture swells influencing wave conditions in the NEA. In contrast, Calvino et al. (2022) employed a nested WW3 model with larger outer domain covering the entire Atlantic to investigate the large-scale processes, such as the NA current, on wave propagation.

WAM considers problems on oceanic scales, and it uses the explicit schemes in space so that it requires small grid size in shallow water, thus making it unsuitable for coastal applications (Bingölbali et al., 2019). SWAN, specifically designed for shallow water processes, is more suitable to simulate wave conditions nearshore in the NEA (Anton & Nash, 2020; Atan et al., 2016; Bento et al., 2011, 2016; Guisado-Pintado, 2020; Neill, 2024; Reduan Atan & Goggins, 2017; Zed et al., 2022). Nesting SWAN within large-scale models such as WAM and WW3 is a common practice. Swain et al. (2019) demonstrated that SWAN hindcasts using WAM boundary conditions generally showed a 5%–15% error compared to deep-water models, yet provided more reliable nearshore wave predictions at buoy locations in the North Indian Ocean, compared to SWAN hindcasts using WW3 boundary conditions. Additionally, the nested WAM-SWAN approach by Lalbeharry and Ritchie (2009) demonstrated that coarse-grid (0.5°) WAM outputs can provide effective boundary conditions for SWAN, enabling accurate simulation of wave transformation from deep to shallow waters. These studies collectively support the nesting approach employed in the present study, which uses WAM and SWAN to capture the full wave spectrum, from swell generation in the open ocean to the wave transformation in shallow coastal waters.

Accurate wave predictions rely heavily on high-resolution wind forcing, as wind serves as the primary mechanism for wave generation (Baordo et al., 2020; Barbariol et al., 2022). The generation of such high-resolution wind data at regional scales typically involves downscaling techniques. Dynamical downscaling employs atmospheric models to enhance the spatial and temporal resolution of wind fields, providing more robust solutions for wave modeling. For instance, Markina et al. (2018) utilized the WRF model to downscale wind fields in the NA, achieving a 14 km resolution to improve wave prediction accuracy in this region. Similarly, HARMONIE mesoscale model was used to dynamically downscale ERA-Interim reanalysis data to 2.5 km resolution for wave hindcasts in Ireland (Gallagher, Tiron, et al., 2016). In Galway Bay (west coast of Ireland), regional weather model, WRF, provided atmospheric forcing for SWAN, further demonstrating the effectiveness of localized wind inputs for wave simulations (Ana Rute Bento & Soares, 2018). While these dynamical approaches significantly enhance the accuracy of wave predictions, their computational demands and resource intensity is still a challenge. On the other hand, statistical downscaling methods have been widely utilized to refine coarse global climate model (GCM) outputs for wave studies. For instance, Weibull-based downscaling techniques (Alizadeh et al., 2020) and multi-step statistical algorithms (Towe et al., 2017) have been applied to improve wind fields for wave climate analysis in the Persian Gulf and the North Sea. However, statistical downscaling often assumes

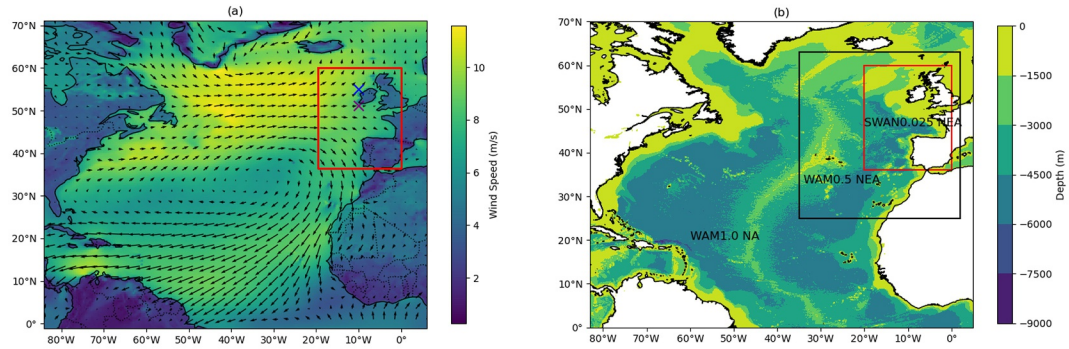

Figure 1. (a) Study region in the North Atlantic, illustrating the mean wind speed (color shading) and direction (black arrows) for 2018 based on ERA5 data. The red box highlights the main area of interest of this study. The blue cross denotes the location of the M4 buoy, while the purple cross represents the M3 buoy. (b) Spatial map of the model domains used in the study. The entire domain represents the WAM1.0NA (North Atlantic) domain, with the black box representing WAM0.5NEA (Northeast Atlantic) domain and the red box representing SWAN0.025 domain. The color shading shows GEBCO bathymetry for the entire region, highlighting variations in seafloor depth.

stationary relationships between large-scale predictors and local-scale predictands, which may limit its applicability under changing climate conditions (Alizadeh et al., 2020).

This paper aims to overcome the limitations associated with low-resolution climate model data and the challenges in downscaling methods by using wind data for wave modeling. For this, we implement an analog approach to generate surrogate wind data for the MPI-ESM (Max Planck Institute of Earth System Model) climate model, utilizing high-resolution ERA5 reanalysis data. The surrogate wind data is used to drive SWAN and WAM wave models in the NEA, with a particular emphasis on Ireland, to explore the wave dynamics for present and future. This approach aims to provide a computationally efficient and accurate framework for studying wave climate variability in dynamic and high-energy coastal regions.

The paper begins with the introduction of the NEA, the primary area of interest (Section 2). To analyze the behavior of waves in this area, wave models are driven by regionally appropriate input data (Section 3). A key aspect of this research is the generation of surrogate wind data to ensure high-resolution wind for wave models (Section 4). The performance of the model is assessed by comparing model results with observational data and sensitivity analyses (Section 5). From this foundation, the research examines the projections of waves both spatially and seasonally with a specific focus on the west coast of Ireland (Section 6). The results are then fully discussed with implications and limitations in Section 7.

2. Study Region

The wind-wave dynamics of the NEA are driven predominantly by westerly and southwesterly winds blowing over the NA ocean (Bertin et al., 2013; Gallagher et al., 2014; Gleeson et al., 2019). Figure 1a illustrates the mean ERA5 wind speed and direction for 2018 for the NA domain, highlighting that most of the wind in the NEA (shown in the red box), particularly around Ireland, is predominantly westerlies. NA swells influenced by wind patterns and mid-latitude cyclones, significantly affect the wave climate around Ireland (Gallagher et al., 2016a; Loureiro & Cooper, 2019). These swells propagates eastward play a critical role in shaping nearshore wave characteristics of Ireland, including significant wave heights and occurrence of extreme wave events (Gallagher et al., 2016b). Analysis of nearshore waves during major storm events in 2015–2017 highlights how these swells contribute to high-energy waves in the NEA, particularly along Ireland's Atlantic coast (Fedele et al., 2019). These waves are further influenced by the complex geomorphology of the Irish coast (O'Brien et al., 2013) and climate phenomena such as the North Atlantic Oscillation (NAO). During positive NAO phase, stronger westerly winds intensify wave heights and increase the frequency of storm events, making the region highly energetic and dynamic (Dodet et al., 2010).

Projections using global climate models such as EC-Earth, indicate a potential decrease in wind speeds over NA by upto 3.5% by the end of the century, which may reduce swell generation and significant wave heights near Ireland (upto 15% in some seasons; Gallagher, Gleeson, et al., 2016a). Similarly, WW3 model predicts decline in

both mean and extreme wave heights, with the most pronounced reductions occurring in winter and summer around Ireland (Gallagher, Gleeson, et al., 2016b). Despite these projected decreases, the variability in wave conditions remains significant. This is due to the region's sensitivity to the NAO phase and interactions between local wind patterns and the Irish coastlines geomorphology.

The western Irish coast, directly exposed to NA weather systems, experiences a wave climate dominated by long-period swells superimposed with locally generated wind waves (Gaughan & Fitzgerald, 2020). This combination, along with the influence of climatic drivers and the extensive fetch of the Atlantic, underscores the importance of understanding wave climate dynamics in the region and its implications for natural and socio-economic systems, particularly in the context of future climate change.

3. Wave Model and Data

3.1. WAM Model

WAM (Günther et al., 1992) is a third-generation model that describes the evolution of wave spectrum by solving wave energy equation. WAM, which is used here with its latest version Cycle 6, is an open-source code developed by the WAMD Group and maintained by the German Institute HZG (Helmholtz-Zentrum Geesthacht; Baordo et al., 2020).

A domain covering the entire NA was chosen to capture the swell waves generated in mid-latitudes. The WAM model, with a spatial resolution of 1.0° × 1.0° (WAM1.0NA), simulates large-scale wave generation and propagation across the Atlantic basin (refer Figure 1b). This model serves as the outer boundary for subsequent nested models, enabling the transition of oceanic waves into more detailed regional and coastal simulations. Daily sea ice concentration was incorporated into WAM1.0NA simulations. As highlighted by Tuomi et al. (2019), the choice of sea ice data source significantly influences the results, irrespective of the method employed. For the current model setup, grid points with an ice concentration exceeding 30% were excluded from model computations. To provide higher-resolution boundary conditions for coastal modeling, one-way nesting technique was applied in the WAM model. A finer-resolution WAM model with spatial resolution of 0.5° (WAM0.5NEA) was set up for the NEA, refining the wave field for regional analysis (black box in Figure 1b represents the WAM0.5NEA domain). This domain covers the waters surrounding Ireland and accounts for the wave transformations that occur as waves propagate from the deeper NA toward the continental shelf. Wave boundary conditions for this domain were supplied by the coarser NA WAM model. However, sea ice was excluded from the WAM0.5NEA simulations, as it was observed only in the Northwest Atlantic, outside the primary domain of interest.

Both WAM models were implemented with 12 directional bins and 25 frequency bands, with the energy balance equation integrated using a propagation time step of 10 min. The lowest frequency resolved was 0.0418 Hz and all other settings were kept to default values. The WAM model simulations were conducted using default ECMWF Cycle 45R1 physics for input and open ocean dissipation (IPHYS set to 0). Wave breaking (BREAK) and the Phillips source function (PHILL) were both set to 0 as the focus was on large-scale wave simulations, these processes are less critical. Depth scaling of the source function (ISLN) was set to 0, making it suitable for deep water conditions (Janssen & Bidlot, 2003).

3.2. SWAN Model

Another third-generation spectral wave model, SWAN, is used to simulate wave climates around Ireland. Though WAM and SWAN have the same scientific principle, SWAN has some additional formulations for shallow water simulations (Lemos et al., 2023; Rusu et al., 2008). SWAN Cycle III 41.45 version is used to set up the regional model for NEA. The current method uses one-way nesting, where WAM0.5NEA model provides wave boundary conditions to the finer SWAN model. This ensures that large-scale wave processes are accurately represented in the coastal model, allowing the high-resolution SWAN model to simulate local wave conditions without feedback loops that would increase computational complexity. The nesting approach dynamically downscales the wave field, ensuring that swell generated in the open ocean is transferred effectively to the regional and coastal models. The SWAN model, with a spatial resolution of 0.025° × 0.025° (SWAN0.025), provides detailed simulations of the wave climate around the Irish coast (red box in Figure 1b represents the SWAN domain). The geographical extent of WAM and SWAN domains along with grid information and inputs used are provided in Table 1. The

Table 1
Computational Grids and Inputs Used for Model Simulations

	Geographical extent				Spatial resolution		Inputs			
Grids	North	South	West	East	$\Delta x \times \Delta y$	$nx \times ny = N$	Wave	Wind	Sea ice	Sea level
WAM1.0NA	69°	0°	−82°	4°	1° × 1°	70 × 87 = 6,090	–	×	×	–
WAM0.5NEA	63°	25°	−35°	2°	0.5° × 0.5°	77 × 75 = 5,775	×	×	–	–
SWAN0.025	60°	36.5°	−19.5°	0°	0.025° × 0.025°	780 × 940 = 733,200	×	×	–	×

Note. Δx: spatial resolution in x direction. Δy: spatial resolution in y direction. nx: number of grid points in x direction. ny: number of grid points in y direction.

model captures the wave transformation processes as waves move into shallow coastal waters, influenced by local bathymetry and coastline features.

SWAN was configured with the same directional discretization as WAM (12 bins), and sensitivity tests showed only minor differences when using higher spectral resolution. So the current SWAN set up consists of 12 uniformly distributed directions and 25 frequencies, which are logarithmically spaced from 0.046 to 1.0 Hz. The SWAN model simulations are run with a non-stationary mode with a 30-min time step. SWAN was run in third-generation mode, incorporating the WESTH (nonlinear saturation-based whitecapping combined with wind input; SWAN Team (2023)) formulation for wind-driven wave growth, the BSBT (Backward Space Backward Time) scheme for wave propagation, and both triad and quadruplet wave–wave interactions. The model included whitecapping and bottom friction to account for wave energy dissipation, and wave breaking was enabled to capture nearshore wave transformations. SWAN default formulations and coefficients were used for all of the physical processes.

3.3. Data

3.3.1. Bathymetry

Two data sets were used for model bathymetry development. GEBCO_2023 (General Bathymetric Chart of the Oceans_2023) grid is a global model for ocean and land that provides elevation data which is available on 15 arc seconds interval grid (GEBCO Bathymetric Compilation Group, 2023). Both WAM models use GEBCO bathymetry interpolated to a 0.5° grid. INFORMAR (Integrated Mapping for the Sustainable Development of Ireland's Marine Resources) maps Irish coastal and offshore waters at resolution ranging from 500 to 2 m and is managed by the Geological Survey of Ireland (GSI) and the Marine Institute (Sheehan, Kevin and INFOMAR Survey Team, 2021). To obtain high-resolution bathymetry near the shore, SWAN uses INFORMAR and GEBCO bathymetry interpolated to a grid of 0.025° resolution.

3.3.2. Wind

The study utilizes two distinct wind data sets: the low-resolution MPI-ESM (Max-Planck Institute of Earth System Model) wind data from the CMIP6 ensemble and the high-resolution ERA5 reanalysis data. To mitigate the limitations associated with the coarse-resolution wind data for wave modeling, we employed ERA5 data as a high-resolution reference for generating surrogates for MPI-ESM wind. This is explained in detail in Section 4.

ERA5 is the fifth-generation of ECMWF atmospheric reanalysis of the global climate (ECMWF, 2019a) which delivers atmospheric, land surface, and ocean wind wave data. Wind components are available at 0.25° (31 km) grid spacing and at an hourly frequency (ECMWF, 2016; Hersbach et al., 2023). This work utilizes 10 m u (u10) and v (v10) components of wind spanning from period 2004 to 2023.

MPI-ESM is a comprehensive climate model used for simulating Earth's climate system and developed by the Max-Planck Institute of Meteorology, Hamburg, Germany (Garcia-Pereira et al., 2023). It couples different components of Earth system including the atmosphere—ECHAM6 (Stevens et al., 2013), ocean dynamics and sea ice—MPIOM (Jungclaus et al., 2013), land surface processes—JSBACH (Reick et al., 2013) and marine biogeochemistry—HAMOCC (Ilyina et al., 2013).

The 10 m u (uas) and v (vas) components of wind used in this study are obtained from first realization (r1i1p1f1) model simulation of the CMIP6 version of Max Planck Institute Grand Ensemble (MPI-GE CMIP6) which is

based on the MPI-ESM version 1.201p7 (Olonscheck et al., 2023). The model includes simulations under five emission scenarios and the data used in the current study corresponds to SSP5-8.5. The low-resolution (LR) configuration, MPI–ESM LR, has a horizontal atmospheric resolution of 1.875° (200 km) and includes 47 vertical layers (Düsterhus & Brune, 2024). For the present study, MPI-ESM LR wind from 2004 to 2023 (representing the present climate) and 2081 to 2100 (representing future climate projections) were used.

3.3.3. Sea Ice

The sea ice model is integrated within the ocean general circulation model MPIOM. It provides daily sea ice concentration on a bipolar grid with a nominal resolution of 1.5° (Jungclaus et al., 2013). To make the sea ice data compatible with the wave models, the data were interpolated to a regular grid of resolution 0.5°. According to recent studies, Arctic sea ice is projected to experience a significant decline by 2100 (Ivanov & Repina, 2018), with the oldest ice potentially disappearing around mid-century (Chen et al., 2021). Chen et al. (2021), further indicate that sea ice thickness is anticipated to decrease at an average rate of 0.22 m per decade after September 2060, accompanied by a comprehensive decline in sea ice concentration and volume. Similarly, Dauner et al. (2024) highlights a long-term decline in sea ice extent in the Greenland and NA sector based on historical data, model simulations, and proxy-based reconstructions, which consistently predict significant reductions in sea ice. Considering these projections, the presence of sea ice in the study region was neglected for the future.

3.3.4. Sea Level

Regional sea level data from the IPCC 6th Assessment Report (AR6) (Fox-Kemper et al., 2021) under SSP5-8.5 scenario was used for the present study. Data are available from 2020 to 2150 along with how these projections differ depending on future scenarios (Kopp et al., 2023). To account for the effects of tide and storm surges, the tide surge anomaly (tideSurgeAnom) from UK Climate Projections 2018 (UKCP18), based on RCP8.5, was added to the regional sea level projection, creating a combined data set that was used in wave modeling. UKCP18 offers updated observations and climate change projections extending to 2100 in the UK and globally (Lowe et al., 2018). Since the UKCP18 data are available on an irregular grid, it was interpolated to a 0.5° regular grid before being integrated with the sea level projections.

3.3.5. Wave Buoy Data

Wave height data from observational buoys (M2-M6) are used to validate the models. These buoys form part of the Irish Marine Data Buoy Observation Network (IMDBON), which is managed by the Marine Institute and Met Éireann, and funded by the Department of Agriculture, Food and the Marine (Marine Institute, 2022). IMDBON provides hourly weather measurements as well as wave height and wave period since 2001.

The locations of the wave buoys are shown in Figure 2 and the distances from shore along with latitude and longitude values are provided in Table 2. Buoy M6, situated off the west coast of Ireland in deep water, was used to validate significant wave height (Hs) outputs from the WAM0.5NA model. The other buoys, M2–M5, are located closer to the shore and were employed for validating the SWAN model. Among these, buoys M3 and M4, positioned along the west coast of Ireland, were of particular interest as this region is directly influenced by NA swells. For further details on the validation process, refer to Section 5.

4. Downscaling Wind via Surrogate Data Generation

Dynamical downscaling of winds, which uses regional weather models to drive wave simulations (Markina et al., 2018) or coupling them with wave models (Bento et al., 2016), is a common approach in wave modeling. Instead, we use an analog method to downscale the climate model output. High-resolution ERA5 reanalysis data are used to generate surrogate winds for low-resolution MPI-ESM. The surrogate winds follow the daily evolution of MPI-ESM and preserve its large-scale spatio-temporal characteristics, while providing realistic high-resolution representation through selected ERA fields. This ensures temporal and spatial consistency between the coarse-resolution driving model and the high-resolution surrogate data.

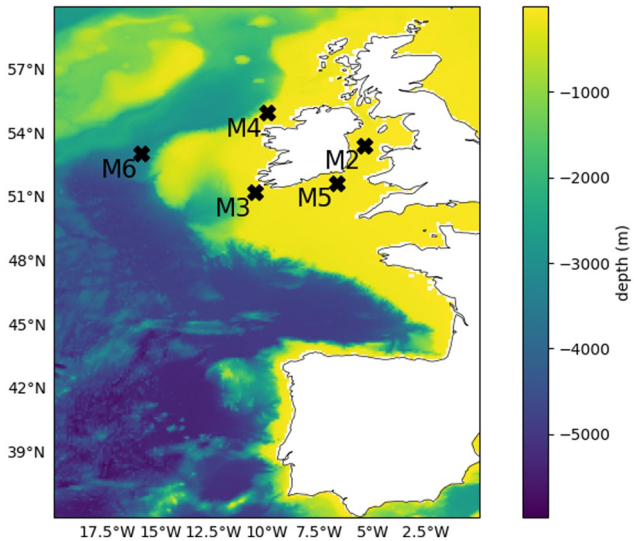

Figure 2. Domain covering SWAN0.025 grid, showing high-resolution bathymetry used for SWAN model set up. The bathymetry is derived from combination of INFOMAR and GEBCO data sets. The locations of Irish observational buoys used for validation are marked (cross) within the domain.

4.1. Analog Method for Surrogate Data Generation

The analog approach used here involves finding analogs or similar instances in a reference data set that match certain characteristics of the target data set. This method relies on identifying the instances from the reference data set that closely resemble the conditions observed in the target data set. Then use the corresponding values from the reference data set as surrogates for the target data set.

In this study, the analog approach is applied to generate surrogate wind data for both present and future MPI-ESM simulations using ERA5 as a reference. The goal is to construct surrogates that retain large-scale structure and long-term trends of MPI-ESM wind while preserving the resolution (both in time and space) of ERA5.

To ensure a consistent comparison during analog selection, it is necessary to bring both data sets to the same spatial and temporal resolution. Accordingly, the ERA5 data, available at 0.25°, is first spatially regridded to match the coarser MPI-ESM grid (1.8°). Then, daily averages of the u10 and v10 are computed from ERA5. This preprocessing ensures that both data sets are aligned in space and time, enabling a direct comparison of wind conditions over a defined spatial domain.

The choice of this spatial domain is a key aspect of the surrogate generation process, as it strongly influences the ability of the selected analogs to reproduce relevant physical conditions. In particular, the spatial domain determines which atmospheric features are prioritized when computing similarity between the target and candidate wind fields. A larger domain may emphasize large-scale wind patterns, while a smaller, regional domain focuses the comparison on localized wind conditions. A detailed discussion on the sensitivity to domain size is provided in Section 5.3.

To identify analogs, the daily wind fields from MPI-ESM are compared with daily averaged wind fields from ERA5. For each target day in MPI-ESM (M_{ref}), a search window of ±14 days around the same calendar day is applied to each year in the ERA5 data set spanning from 2004 to 2023. This rolling 29-day window across 20 years resulted in a candidate pool of 580 ERA5 days (E_n, $n = 1, 2, \ldots, N$; N is the total number of candidates) for each M_{ref}. This approach balances the need for seasonal consistency with sufficient variability in candidate patterns.

The similarity between M_{ref} and E_n was quantified using vector difference (VD) in wind components. Specifically, the Euclidean distance (Senter & Lupo, 2024) between the wind vectors was computed at each grid point using the formula:

Table 2
Statistical Results of Hs at Each Locations

					Hs from WAM0.5NEA				
	Lat (°)	Lon (°)	Distance from Irish shore (km)	Bm	Sm	Bias	RMSE	SI	r
M6	52.986	−15.866	389	3.912	3.514	−0.397	0.768	0.196	0.766
					Hs from SWAN0.025				
	Lat (°)	Lon (°)	Distance from Irish shore (km)	Bm	Sm	Bias	RMSE	SI	r
M3	51.217	−10.550	56	3.656	3.427	−0.229	0.627	0.171	0.871
M4	55.000	−10.000	83	3.742	3.519	−0.223	0.528	0.146	0.867
M2	53.480	−5.425	37	1.671	1.527	−0.143	0.419	0.250	0.899
M5	51.690	−6.704	56	2.717	2.552	−0.165	0.570	0.209	0.922

Note. Bm: mean Hs from buoy, Sm: mean Hs from model simulations, RMSE: root mean square error, SI: scatter index, *r*: Pearson's Correlation Coefficient.

$$VD_n = \sqrt{(M_{ref_u} - E_{n_u})^2 + (M_{ref_v} - E_{n_v})^2}, \quad n = 1, 2, \ldots, N$$

where $N = 580$, depending on data availability (e.g., leap year).

The VD field then quantifies the difference between MPI-ESM and ERA5 wind vectors at each grid point. The VD field is then spatially averaged over the domain to obtain a single similarity score for each candidate day. The ERA5 day with the minimum spatially averaged VD is selected as the best analog for the corresponding M_{ref}. The schematic diagram Figure 3 illustrates the process of analog selection for MPI-ESM surrogate generation. An advantage of using the vector difference as the similarity metric is that it inherently captures both wind speed and wind direction differences, thereby simplifying the similarity assessment while still retaining the full vector characteristics of the wind field.

Once the best analog day is identified for each MPI-ESM day, the corresponding high-resolution wind fields from ERA5 ($u10$ and $v10$) were extracted. These extracted wind fields are then connected in temporal order to construct a continuous high-resolution surrogate wind time series. As the analog days are selected based on daily similarity to MPI-ESM wind fields, the resulting sequence of surrogate days reflects the trends and variability embedded in the original MPI-ESM simulations, while attaining spatial and temporal resolution of ERA5.

As an example, consider 18 January 2081, from the MPI-ESM simulation. A ±14 day search window is applied around this date, spanning from January 4 to February 1. All dates within this window are extracted from each of the 20 years in the regridded ERA5 record (2004–2023), resulting in a total of 580 candidate days. For each candidate day, the spatially distributed vector difference between the MPI-ESM and ERA5 wind components is computed, and the mean VD over the domain is calculated. Suppose 22 January 2007, is identified as the day with the minimum spatially averaged VD; this day is then selected as the best analog for 18 January 2081.

If 3-hourly ERA5 wind data are used as the high-resolution reference, then the full 3-hourly wind fields from the selected analog day (in this case, 22 January 2007) are used as the surrogate wind input for the MPI-ESM target day. This process is repeated for each day in the MPI-ESM time series, resulting in a surrogate data set with the resolution of ERA5 and the large-scale variability of the MPI-ESM simulation.

Using the same ERA5 data set for both present and future scenarios offers a consistent baseline, reducing the risk of introducing biases that could arise from using different data sets. While this method assumes that present-day ERA5 variability is a reasonable proxy for the structure of future variability, it is a standard and robust approach in climate modeling, especially when high-resolution observational data sets for the future are unavailable. A similar approach was employed by Noël et al. (2021), who performed statistical downscaling of CMIP5 projections using ERA5 as a reference data set. In their study, they statistically downscaled historical data, validated it against ERA5, and used the identified biases to correct the projected downscaled data. This demonstrates the viability of using ERA5 as a reliable baseline for generating high-resolution data and correcting model biases, further supporting the assumption that present-day ERA5 variability can serve as a reasonable proxy for future scenarios in surrogate data generation.

5. Model Validation and Sensitivity Analysis

In this section, the two experiments—validation and temporal sensitivity analysis—are conducted using real wind data from ERA5 to assess the model's ability to represent current conditions. The validation involves computing the statistical matrices of model outputs driven by high-resolution ERA5 winds against observed data. Following this, a sensitivity analysis examined the impact of wind data resolution by comparing model performance using high to low-resolution wind inputs. Based on the conclusions drawn from this analysis, a second sensitivity experiment is carried out using surrogate winds generated by selecting different domain for computing VD between the climate model and reanalysis data.

5.1. Model Validation Against Observational Buoys

The study area chosen benefits from a dense network of in situ buoy observations (refer Figure 2 for locations). The validation period from 21 September 2023 to 10 October 2023 was carefully chosen to ensure the availability of continuous, error-free observational data, thereby eliminating potential uncertainties associated with data gaps

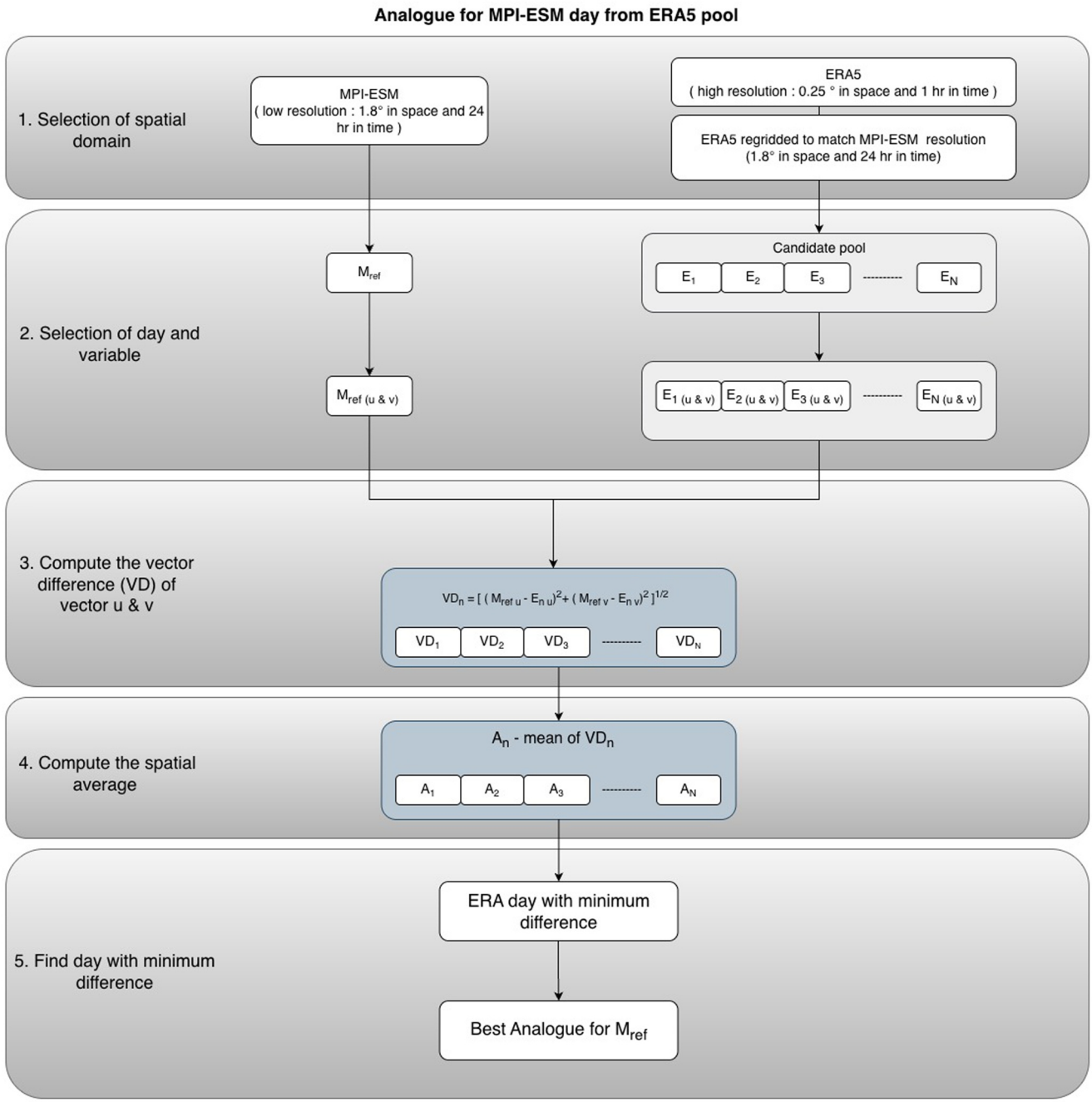

Figure 3. Schematic representation of analog finding for the surrogate wind data generation. The method integrates coarser MPI-ESM and fine ERA5 data. The process begins with selecting the spatial domain, after which data sets are regridded and resampled to ensure consistent spatial and temporal resolution. For selected day in MPI-ESM (M_{ref}), the vector difference (VD_n) between ERA5 ($E_{n(u\&v)}$) and MPI-ESM ($M_{ref(u\&v)}$) wind components is computed over the selected domain. The spatially averaged vector difference (A_n) is then used to identify the ERA day with minimum difference, which is selected as best analog.

or inaccuracies. For this simulation period, model outputs were saved at hourly intervals to allow for detailed temporal comparison with observations.

Statistical validation of modeled Hs against buoy observations was undertaken to understand the skill of models WAM0.5NEA and SWAN0.025. The computed statistics of Hs (refer Table 2) are the mean of measurements (Bm) and model simulations (Sm), the bias, the root mean square error (RMSE), the scatter index (SI) and the Pearson's Correlation Coefficient (r).

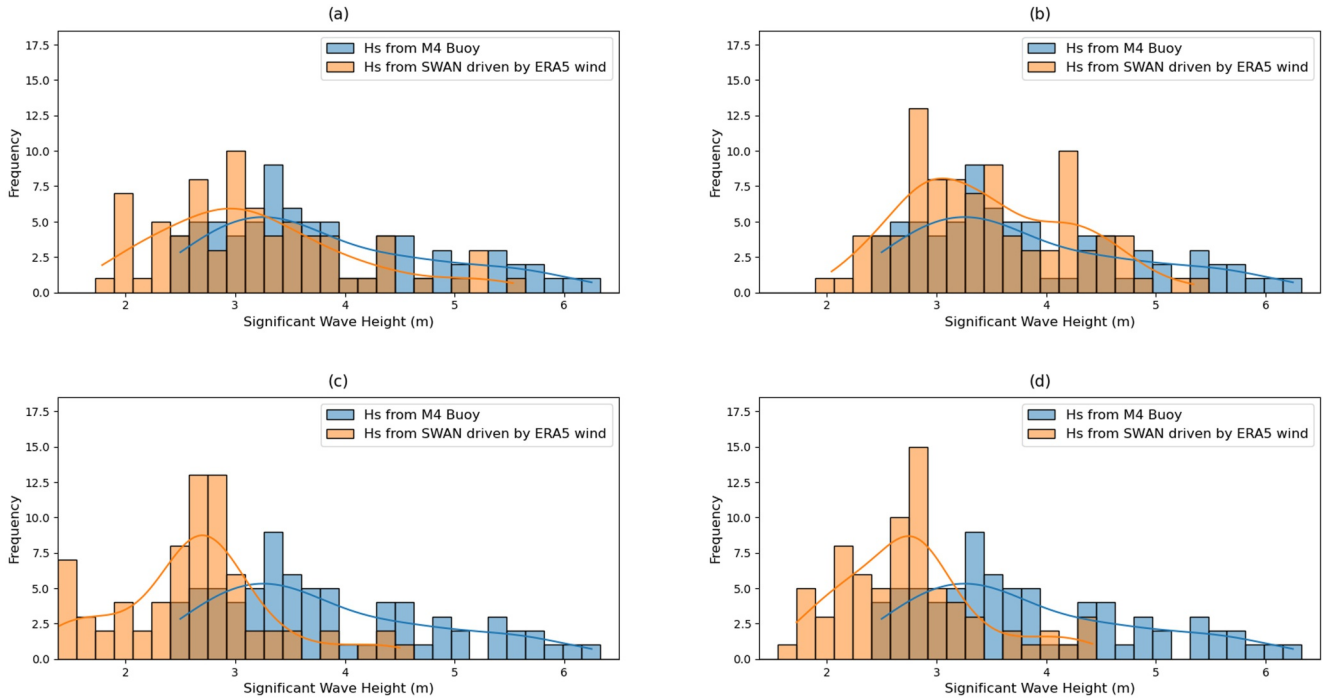

Figure 4. Comparison of Hs distribution from SWAN driven by ERA5 winds having temporal resolution of 1 hr (a), 3 hr (b), 6 hr (c) and 24 hr (d) with significant wave height from M4 buoy. The blue line represents the distribution curve of Hs from M4 buoy, while the orange line represent the distribution curve of Hs from SWAN0.025 model. The blue bars indicate the wave height distribution derived from M4 buoy while the orange bars indicate the wave height distribution derived from the model simulations.

The locations on the west coast of Ireland (M6, M4, and M3), directly influenced by NA swells, exhibit higher mean Hs than the locations on the east coast of Ireland (M2 and M5) during the validation period. In contrast, M2 and M5, which are sheltered from the direct influence of swells and dominated by wind-sea conditions, have different statistical characteristics than M6, M4, and M3. Negative bias across all locations suggests that the model tends to underpredict Hs than the observations, with higher bias on the west coast locations where the influence of swell is stronger. RMSE follows a similar pattern with higher values on the west coast. The lower bias and RMSE on the east coast reflects the dominance of local wind-driven waves. Conversely, the lower scatter index (SI) on the west coast indicates that the model predictions are more consistent for swell-dominated locations but show greater variability (high SI on the east coast) in regions where wind-driven waves dominate.

Correlation coefficients (r) further support these findings, with the highest correlations observed on the east coast (M5: 0.922, M2: 0.899) and slightly lower values on the west (M3: 0.871, M4: 0.867, M6: 0.766). The strong correlation across all locations suggests that the model successfully captures temporal variations in wave height.

5.2. Sensitivity to Temporal Resolution of ERA5 Wind Forcing

Simulations, similar to the validation period, were conducted by driving WAM-SWAN setup using ERA5 wind data at different temporal resolutions–1, 3, 6, and 24 hr–to assess the influence of wind forcing on wave model performance. Most studies focus on the matching of waves and extreme events. However, our focus is on the full distribution of wave heights along the Irish coast, as it provides valuable insights for adaptation strategies. The Hs distribution from SWAN0.025 simulations, driven by ERA5 winds, was compared to observations from the M4 buoy. The results, as illustrated in Figure 4, indicated good alignment of distribution curve of Hs from model (blue lines) with observations (orange lines) for 1-hourly and 3-hourly wind data, while significant deviations were noted with 6-hourly and daily forcings. Also, the models successfully reproduced the frequent waves with heights ranging between 2.5 and 4 m when driven by hourly and three-hourly wind forcing. However, this was not achieved with six-hourly and daily wind forcing.

Table 3
Summary of Data Inputs for Wave Simulations, Resolution of Input Data, and Agreement of Model Hs With Observations

	Input data	Temporal resolution (hr)	Spatial resolution (°)	Buoy used for comparison	EMD (buoy vs. model Hs)
Phase I	ERA5	1	0.25	M4	0.656
	ERA5	3	0.25	M4	0.386
	ERA5	6	0.25	M4	1.449
	ERA5	24	0.25	M4	1.083
Phase II	VD-NA	3	0.25	M3	0.156
	VD-NEA	3	0.25	M3	0.146
	VD-Ireland	3	0.25	M3	0.091
	VD-NA	3	0.25	M4	0.173
	VD-NEA	3	0.25	M4	0.129
	VD-Ireland	3	0.25	M4	0.103

Note. In Phase I, 3-hourly ERA5 (highlighted in gray) wind was chosen for surrogate wind data generation in Phase II. In Phase II, the model was driven using surrogate winds generated from different domains selected for computing vector difference, and the model performance was compared. VD-Ireland (gray rows) was selected for our study. *VD-NA*: Surrogate data generated by computing vector difference between MPI-ESM and ERA5 winds over the North Atlantic. *VD-NEA*: Surrogate data generated by computing vector difference over the Northeast Atlantic. *VD-Ireland*: Surrogate data generated by computing vector difference over a domain around Ireland.

To quantitatively assess the similarity between modeled and observed wave height distributions, the Earth Mover's Distance (EMD) was computed for model Hs from each wind forcing case with the buoy Hs. EMD is a metric used to compare two distributions (Düsterhus & Hense, 2012; Luzia et al., 2022). It measures the effort required to transform one distribution into another by considering the amount and distance of "mass" that must be shifted (Luzia et al., 2022). The results provided in Phase I of Table 3 revealed that 3-hourly forcing produced lower EMD value (0.38), indicating closest match to the observed distribution. Although model results from the 1-hourly wind forcing appeared visually similar to observation, it has higher EMD than 3-hourly wind forcing because the metric captures even small shifts across the full distribution. The 6-hourly and 24-hourly wind forcing produced higher EMD values (1.44 and 1.08), reflecting their inability to reproduce the observed Hs distribution accurately. Considering these findings, along with computational and storage requirements, we selected 3-hourly ERA5 data for generating surrogate winds for MPI–ESM simulations.

5.3. Sensitivity to Spatial Domain Selection for Surrogate Winds

To investigate the influence of spatial domain selection (represented as the first step in the schematic diagram Figure 3) on surrogate wind quality on wave model performance, surrogate data sets were generated using three different domains: the full NA, the NEA region consistent with the WAM0.5NEA domain and the region around Ireland matching SWAN0.025 model. In all cases the high-resolution surrogate wind fields were generated by rearranging 3-hourly ERA5 wind data from the entire NA, based on time indices identified through analog matching. The resulting surrogate wind forcing was then used to drive the nested model system to simulate wave conditions for the year 2023. The modeled daily Hs from SWAN for each experiment was compared against observations from the M3 and M4 buoys. Model performance was also evaluated by calculating the EMD between the modeled and observed Hs distribution at both locations.

The wave height distribution curves, as shown in Figure 5, from three different model simulations appear to be similar to observations. However the surrogate wind generated using the domain around Ireland resulted in closest match. This is further supported by the EMD values, which were lowest at both buoy locations (0.09 at M3 and 0.1 at M4) when the wave models were driven by VD-Ireland wind field. These results highlight that selecting analogs based on local wind conditions can significantly improve model performance in the nearshore region around Ireland.

The experiments described above determine the final model set up in this study. Using ERA5 winds, the validation against buoy observations demonstrates that the nested WAM-SWAN framework can reproduce observed wave conditions in the Irish waters with reasonable accuracy. The sensitivity analyses further indicate that 3-hourly wind forcing provides the best representation of the full distribution of significant wave heights, and that

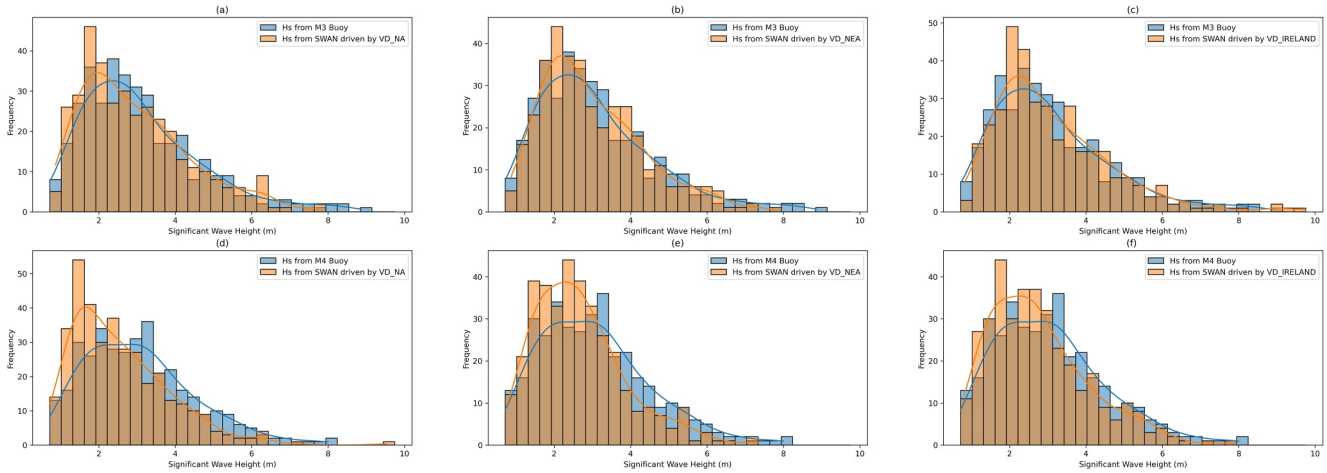

Figure 5. Comparison of significant wave height distribution from SWAN driven by surrogate winds generated through selecting different domain with significant wave height from M3 and M4 buoy. The blue line represents the distribution curve of Hs from buoy and the orange line represent the distribution curve of Hs from SWAN0.025 model driven by VD-NA winds (a and d), VD-NEA winds (b and e), and VD-Ireland winds (c and f). The top three plots represent comparison of model Hs with M3 buoy and bottom three for that with M4 buoy. The bars indicate the histogram of wave heights from buoy and model.

selecting analogs based on the Ireland domain produces surrogate wind fields that generate realistic wave conditions. Based on these findings, 3-hourly wind data and the Ireland domain were selected for generating surrogate winds. These surrogate winds, derived from climate model data, are used to simulate wave conditions to examine the present and future wave climate around Ireland. While biases exist in climate model winds, the focus of this study is the relative differences between present and future simulations, rather than the absolute magnitude of wave heights.

6. Wave Projections in the Northeast Atlantic

A 20-year simulation (2004–2023) was conducted to represent the present wave conditions, using surrogate data generated under a high-emission scenario (RCP8.5). Sea ice was included in the NA (WAM1.0NA) model to capture its influence on wave propagation to the inner domain and sea level, consistent with the same emission scenario, was incorporated into the SWAN model to account for its effects. To evaluate changes in the wave climate, the present simulation was compared with a 20-year projection (2081–2100), also under RCP8.5. The surrogate wind data generated for the future scenario was used to drive the wave models. In the present condition, sea ice was observed only in the northwest Atlantic within the WAM1.0NA domain. Considering the projections from previous studies (Chen et al., 2021; Dauner et al., 2024), sea ice was set to zero in the future simulations to reflect its expected absence under future climate conditions, while projected sea level was included in SWAN simulations.

6.1. Spatial Variation of Wave Height for the Northeast Atlantic

The analysis of Hs differences between future and present conditions, based on a 20-year mean and seasonal averages, reveals notable spatial variations across the NEA under high emission scenario. These variations can be directly related to the projected changes in wind patterns, which are the primary drivers of wave dynamics.

The spatial variation of 20-year mean Hs differences (Figure 6) indicates a significant increase in wave heights in the northern part of the domain, mainly in the northwest of Scotland and the west of Ireland. This is likely driven by stronger and more persistent westerly winds associated with a general poleward shift in storm tracks and intensified mid-latitude cyclones (Gentile et al., 2023; Pinto et al., 2013).

In contrast, a reduction in Hs is observed primarily in the central part of the domain, particularly in the mid-latitudes of the NEA. These areas show a broad but moderate decrease in wave heights, which may be attributed to the shift in storm trajectories. The Iberian Peninsula exhibits relatively stable conditions, with minimal change in Hs compared to the present, indicating little impact from projected wind changes in this region. The semi-enclosed seas such as the Irish Sea and the English Channel show a slight reduction in Hs. The change in

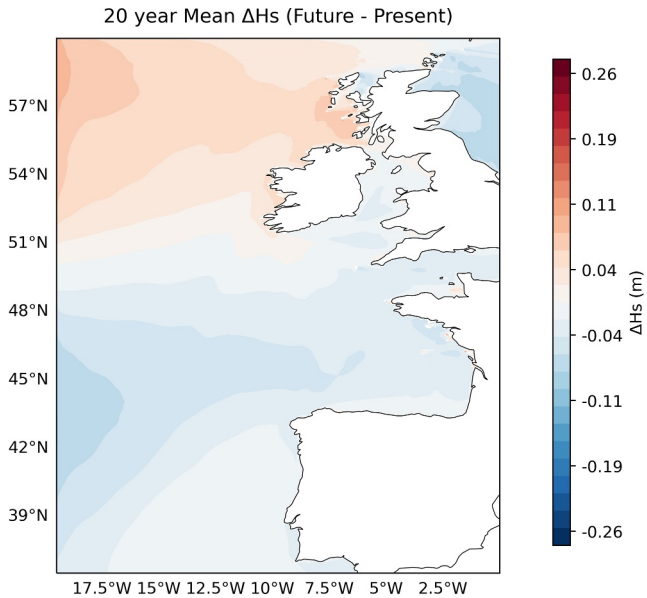

Figure 6. Spatial difference in the 20-year mean significant wave height (Hs) for the Northeast Atlantic between future (2081–2100) and present (2004–2023) conditions. Positive values (red) indicate an increase in wave height, while negative values (blue) indicate a decrease, highlighting regional variability in projected wave climate changes.

these area is smaller than in the central open ocean, possibly due to the influence of local wind dynamics and the sheltering effect of surrounding landmasses.

Earlier studies have shown that the NEA is a region with strong seasonal variations in Hs (Gallagher et al., 2016a; Tiron et al., 2013). Our analysis also reveals pronounced seasonal differences under future climate conditions: winter and summer show increased Hs, spring shows only minor changes, and autumn shows a marked reduction in Hs. Quantitatively, the largest seasonal increase reaches up to 22 cm in winter and the strongest decrease of about 26 cm in autumn. Figure 7 illustrates these seasonal differences and highlights the associated spatial patterns across the NEA domain.

During winter, a pronounced increase in Hs is visible across the northern and western parts of the domain, indicating stronger wave conditions likely associated with intense and frequent winter storms. The region around Ireland shows a widespread increase in Hs under future conditions. Additionally, the Irish sea shows noticeable increase in Hs, suggesting enhanced local wind forcing or greater wave penetration from the adjacent open Atlantic. In spring, the changes are minimal. Most areas show weak positive or negative differences. This suggests that spring will bring relatively stable wave conditions in the future. Summer shows a moderate increase in Hs in the northern and southern parts of the NEA, while the central part shows reduction. Notably, the western Iberian Peninsula, the area near the northen Ireland, and waters west of the outer Hebrides experience higher Hs increases in summer than in winter, highlighting the influence of seasonal wind shifts or persistent local wind forcing during this time. In contrast, autumn shows a widespread and significant decrease in Hs, especially across the central and southern parts of the domain, including west of the Iberian Peninsula and the Bay of Biscay. This is the only season showing a strong and consistent negative anomaly across a broad area, suggesting a notable weakening of wave-generating conditions during this period.

6.2. Localized Changes in Wave Height Along the West Coast of Ireland

To understand how wave height distributions change locally, we compare the distributions of Hs at the locations where the M3 (southwest of Ireland) and M4 (northwest of Ireland) buoys are deployed (hereafter $M3_L$ and $M4_L$ will be used to represent the locations where M3 and M4 buoys are deployed). The analysis compares the present and future Hs, using histograms to examine the wave height distribution and analyzing the differences in bin frequencies and cumulative sum of Hs to provide insights to shifts in wave height characteristics. This helps to identify whether future conditions involve more frequent high waves, changes in moderate wave occurrences, or shifts in calm conditions.

The analysis of wave height distributions at $M3_L$ and $M4_L$ shows notable differences between present (2004–2023) and future (2081–2100). Histograms at both locations (refer Figure 8a, for $M3_L$ and Figure 8c for $M4_L$) reveal contrasting trends. At $M3_L$, the orange bars (future Hs) are generally taller than the blue bars (present Hs) for Hs < 2 m, while the blue bars are mostly taller for moderate waves (2–4 m). But for high waves, from 4 to 8 m, the number of blue and orange bars alternating each other is roughly equal, making it difficult to identify a clear pattern within that range. Few orange bars appear above for Hs > 8 m at $M3_L$. In contrast, at $M4_L$, blue bars are taller than orange bars below 1.5 m, while from 1.5 to 4 m, the orange bars gradually increase and become taller. For higher waves, $M4_L$ shows a pattern similar to what is observed at $M3_L$, and above 8 m, orange bars are present but shorter than blue bars.

It is important to note here that the increase and decrease in each bin are not entirely consistent within a given range. The trend described for each range is based on the majority of bins being taller in either the present or future distribution, rather than every single bin within that interval. While the histograms provide a visual summary of these differences, they do not capture the full picture. The gray lines in Figures 8b and 8d, which represent the bin-to-bin frequency differences, capture these fluctuations; they are often noisy and difficult to interpret. To better

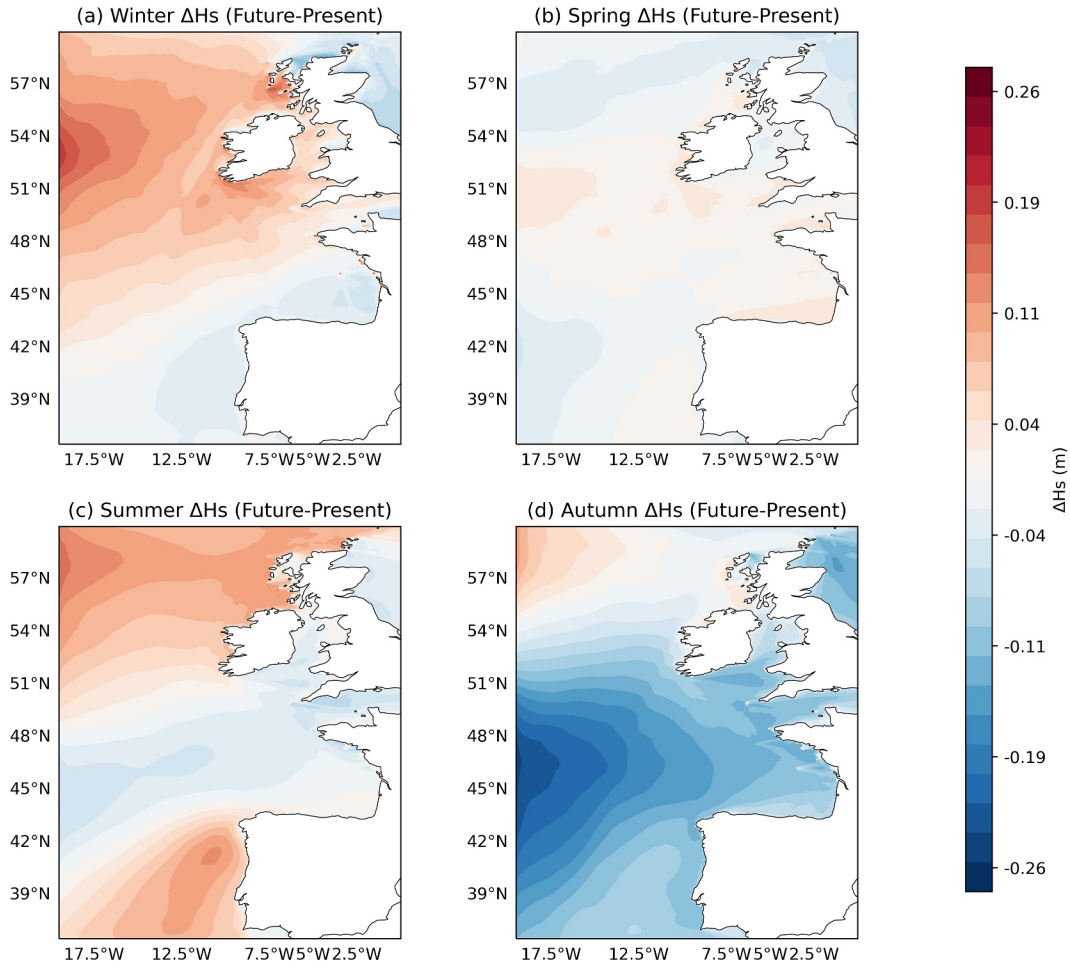

Figure 7. Seasonal differences in the mean significant wave height (Hs) between future (2081–2100) and present (2004–2023) conditions for the Northeast Atlantic. Each panel represents a season (a—Winter, b—Spring, c—Summer, d—Autumn), with positive values (red) indicating an increase and negative values (blue) indicating a decrease in Hs. The plots highlight the seasonal variability in projected wave climate changes.

highlight the overall shift between present and future distribution, the black cumulative sum difference line was included.

At $M3_L$ (Figure 8b), there is a net positive shift below 2 m confirming that calm conditions are projected to become more frequent. A dip across the 2–4 m waves indicates a net reduction in moderate wave heights except around 3 m, where the dip is less pronounced. Interestingly, the black line also reveals a distinct pattern for higher waves at $M3_L$ that was not easily visible in the histogram plot. The line shows a decline from 4 to 6 m followed by a rise from 6 to 8 m suggesting a redistribution within higher wave categories. The curve then flattens after 8 m, highlighting slightly increased extremes.

At $M4_L$ (Figure 8d), the cumulative curve shows a sharp decline for calm conditions and a steady increase for the moderate range. While the curve drops below zero, this does not indicate that wave heights are decreasing overall. Instead, it shows that the future has fewer calm wave events compared to the present. As we move from Hs > 2 m, the curve starts to rise, meaning that moderate waves become more frequent in the future. Overall, the plot reflects a shift in the distribution, where calmer conditions reduce, and moderate wave activity increases. A flatter curve afterwards confirms that extreme conditions remain stable or slightly decrease.

Altogether, at $M3_L$, wave conditions are shifting toward both calmer and more energetic extremes with a reduction of moderate waves. $M4_L$ shows fewer calm states and a modest increase in moderate waves and stable extreme wave frequencies in future. The shifts toward moderate to high waves at $M4_L$ and those toward calm

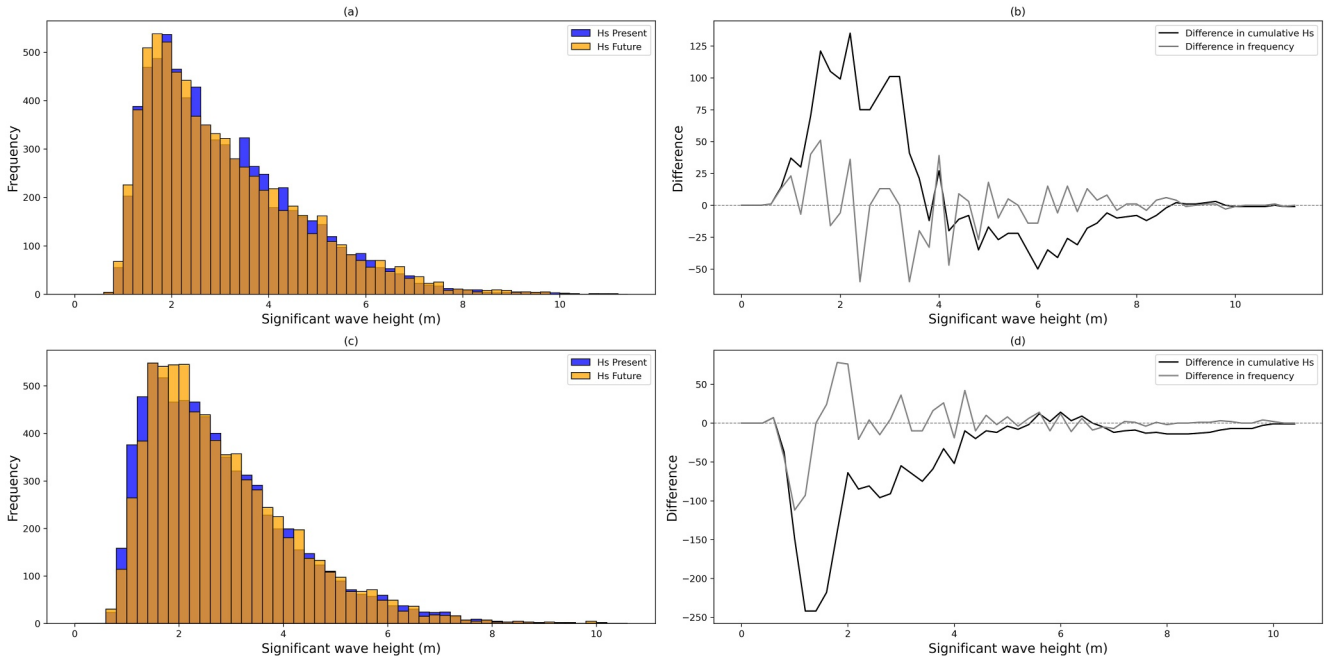

Figure 8. Distribution of Hs and comparison of future and present Hs at $M3_L$ and $M4_L$. The histogram plot (a) shows the comparison of Hs at $M3_L$ for present (blue) and future (orange), while in (b) gray line represents the difference (Future–Present) in bin frequencies of Hs and black line represents the difference in cumulative sum of Hs. Like wise histogram plot (c) shows the comparison of Hs at $M4_L$ for present (blue) and future (orange), while in (d) gray line represents the difference (Future–Present) in Hs and black line represent the difference in cumulative sum of Hs.

waves at $M3_L$ are in line with the 20-year mean Hs difference, which clearly shows greater wave activity in the northwest of Ireland compared to the southwest.

Expanding on the histogram-based analysis, the seasonal cumulative differences at $M3_L$ and $M4_L$ provide a detailed view of how wave height distributions vary across different seasons. The seasonal cumulative differences of Hs between future and present conditions at $M3_L$ (Figure 9a) and $M4_L$ (Figure 9b) reveal distinct patterns in wave height distributions. At $M3_L$, seasonal cumulative differences reveal distinct patterns across wave height ranges. In summer, calmer waves (Hs < 2 m) are more frequent in future, while moderate waves (2–4 m) show a decline, and those between 4 and 6 m (high waves) remain relatively stable. No extreme waves are observed in summer at $M3_L$. During autumn, there is an increase in waves between 1 and 3 m, indicating a shift to calmer than moderate conditions. However, the difference decreases between 3 and 6 m, while higher waves (above 6 m) show very little increase in the future, with the presence of extreme waves (>8 m). In spring, a similar pattern to autumn is observed, with an increase between 1 and 3 m, followed by a decline up to 6 m. However, the magnitude

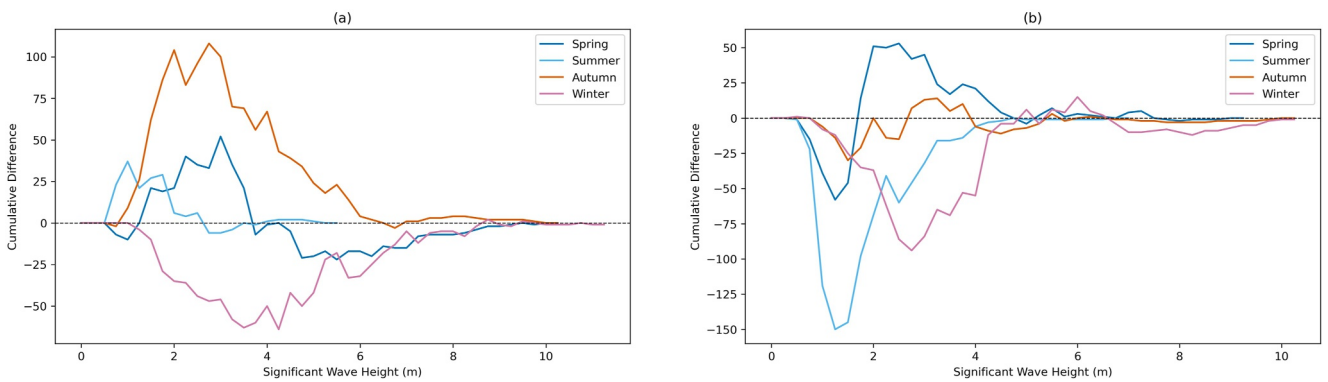

Figure 9. Seasonal difference in cumulative Hs between future and present scenarios at locations $M3_L$ (a) and $M4_L$ (b). The blue line represents spring, sky blue line represents summer, the orange line represents autumn and the pink line represents winter.

of these changes is less pronounced. Unlike in autumn, high waves above 6 m are expected to be more frequent in spring. Winter, in contrast to other seasons, shows a negative cumulative difference for calm to moderate waves, indicating reduced frequency of these events, while the occurrence of higher and extreme waves (>6 m) increases. This suggests a shift toward more energetic wave events during winter at $M3_L$.

At $M4_L$, small waves are projected to decrease in all seasons. In autumn, minimal changes are seen across all wave heights marking a contrast to autumn at $M3_L$, except for extreme waves, which will remain similar to present conditions. Moderate waves become more frequent in spring, with higher and extreme waves showing little changes than present. Summer at $M4_L$ shows an opposite trend to $M3_L$, with a sharp increase in moderate waves and some high waves up to $\sim$7 m, suggesting more energetic conditions. Winter indicates an increase in moderate waves, as well as rise in occurrence of high waves and some extreme events in the 8–10 m range.

7. Discussion

Understanding future wave changes is crucial for long-term coastal planning and management. Global climate models (GCMs), serve as the primary source of future atmospheric forcing. However, because of their coarse spatial resolution (typically ranging from 100 to 250 km grid scales), traditional GCMs, like MPI-ESM, have difficulty in adequately representing small-scale wind variability. To address this, various downscaling approaches, such as dynamical downscaling, statistical downscaling, and, more recently, machine learning-based methods, have been developed.

Dynamical downscaling offers detailed physical representations. However, it is computationally intensive, requiring significant storage and long simulation times (Rozoff & Alessandrini, 2022). In contrast, statistical methods are computationally efficient but rely on predefined relationships, which may limit their ability to capture complex, non-linear interactions between variables (Rozoff & Alessandrini, 2022). According to Zhang et al. (2024), machine learning-based approach models intricate, non-linear relationships and effectively handle high-dimensional data sets. However, they demand significant computational resources, large training data sets, and domain expertise, which can pose challenges for practical implementation (Getter et al., 2024).

This study employs an analog-based approach as a simpler and more resource-efficient alternative. By selecting analog days based on average vector difference with MPI-ESM wind and rearranging high-resolution ERA5 data, the surrogate wind data set preserves the temporal evolution of the climate model while achieving both spatial and temporal coherence of ERA5. In addition, this method captures the non-linear dynamics in the observational data set and preserves the physical realism. Hence, the method adopted overcomes the limitations of traditional statistical methods that often rely on empirical fits or treat grid points independently. Additionally, by using existing data sets and rearranging them based on identified analogs, rather than generating new data through complex simulations or extensive model training, this method aligns with the principles of surrogate modeling—a concept commonly used in machine learning (Bocquet, 2023). Surrogate models simplify complex systems, enabling faster predictions without the need for full simulations (Bocquet, 2023). Similarly, the analog approach effectively generates high-resolution surrogate data using statistical techniques. Thus, the method avoids the computational demands of dynamical downscaling and machine learning while providing reliable inputs for wave climate analysis. Furthermore, considering that machine learning methods often fail to outperform simpler interpolation techniques, such as bicubic interpolation, in reconstructing extreme wind conditions (Rezvov et al., 2022), the analog-based approach provides a computationally efficient and reliable solution for downscaling winds for nearshore wave modeling.

Model validation, sensitivity analysis, and projected wave height changes provide a detailed understanding of the wave climate in the study area under the current and future scenarios. Validation of models against buoy observations confirms that both WAM (WAM0.5NAE) and SWAN (SWAN0.025) adequately capture wave climate, but their performance varies depending on the locations. WAM model was effective in capturing wave dynamics in deep water, its limitations near the shore underscore the need for models like SWAN to resolve fine-scale features. The accuracy of SWAN in representing nearshore wave characteristics further reinforces its suitability for coastal applications, especially in regions having complex geomorphology like the Irish coast. Consistent with this, the comparisons between WAM and SWAN simulations showed that SWAN reproduces wave height variability more accurately at locations closer to the Irish shelf (e.g., M3 and M4) while differences between the two models are smaller at the more offshore location M6.

The sensitivity of SWAN to the temporal resolution of ERA5 wind forcing underscores the importance of high-frequency wind data for accurate wave simulations. The significant deviations observed with 6-hourly and daily wind forcings highlight the inability to resolve the temporal variability needed for reproducing moderate and frequent waves. This finding aligns with the study by Bauer and Weisse (2000), which demonstrated that wave models driven by coarser winds (temporal resolution) significantly underestimate significant wave height. The EMD values computed in this study further strengthen this. The model performance with 1-hourly and 3-hourly wind forcings aligns with the previous studies, reinforcing the decision to use 3-hourly wind data for surrogate wind generation. This decision balances computational efficiency and model accuracy, critical for long-term simulations.

The choice of spatial domain is an important part of the surrogate data generation process, as it affects how well the selected analogs represent the target conditions. The domain should be chosen based on the specific goals of the study. In this study, the surrogate wind data are used to drive wave models. So, it is important to make sure that the selected domain captures the wind patterns that generate waves affecting the region of interest.

Even when the analog selection was based on a smaller region around Ireland, the resulting surrogate winds were created by shuffling ERA5 data covering the full NA, using the selected time indices. Since the prevailing winds reaching Ireland are westerlies, the regional domain inherently reflects large-scale atmospheric patterns over the NA. This means that even though the analog selection is done from a smaller area, the chosen time indices can reflect the larger weather patterns. Preserving large-scale wind effects is crucial for simulating waves near Ireland, as swells significantly shape the Irish wave climate (Gallagher et al., 2016b; Gaughan & Fitzgerald, 2020). The good agreement (low EMD value) achieved by SWAN model nested in WAM forced by the same surrogate wind suggests that the surrogate data not only reproduced the local wind conditions but effectively captured the large-scale wind patterns over the NA basin, which are also responsible for the waves along the Irish coast.

The Euclidean distance between MPI-ESM and EAR5 wind fields computed using the vector components of wind allowed to incorporate both wind speed and direction in similarity assessment. For each day in MPI-ESM, the analog was identified as the day in ERA5 having minimum spatially averaged vector difference. Following this, the 3-hourly wind data were rearranged according to the new time sequence derived from the comparison.

Since ERA5 data are only available up to the present, we used the same reference period (2004–2023) to generate surrogates for both present and future scenarios. However, this does not imply that the same winds represent both time periods. Instead, ERA5 days were selected based on their similarity to MPI-ESM wind patterns for the present and future, allowing the surrogate wind fields to reflect the projected climate signal while maintaining high-resolution physical realism. Furthermore, the MPI-ESM simulations used in this study project generally lower or comparable wind magnitudes in the future relative to the present. This reinforces that ERA5 provides a sufficiently broad range of wind events and remains a valid and appropriate source for analog selection under projected future conditions.

The future projections show noticeable spatial variations in wave height changes across the NEA under the RCP8.5 scenario. An intensification of wave activity observed in the northern parts of the domain, while the southern and eastern regions experienced a reduction in wave heights. These changes can be linked to the influence of shifting wind patterns. The NEA region around Ireland exhibits contrasting trends, with the west coast showing an increase in mean significant wave height, while the east coast remains more stable. Seasonal variations in wave height changes provide additional insights, with the most pronounced increases occurring in winter (up to 22 cm) and summer (up to 15 cm), while autumn exhibits the largest decrease in wave height (up to 26 cm).

However, these findings contrast with those of Gallagher et al. (2016a, 2016b), which projected an overall decrease in Hs, with the greatest reductions occurring in winter and summer under the RCP8.5 scenario near Ireland. Gallagher et al. (2016a) conducted a 30-year future projection compared with a 30-year hindcast of wind-waves using WAVEWATCH III (WW3) and wind data from the EC-Earth global climate model. In contrast, our study focuses on a 20-year comparison of future projections with present conditions, incorporating present and future sea level rise scenarios. The seasonal variations in wave heights follow a pattern similar to the seasonal differences in 20-year mean wind patterns between the future and present from surrogate data. This similarity confirms that the NEA waves are predominantly wind-driven.

In the NEA, where the prevailing winds are predominantly westerlies, surrogate winds generated through the analog method effectively captured the seasonal variations in wind seen in MPI-ESM. The resemblance of

seasonal wave patterns with wind variations also demonstrates the robustness of the approach in regions with relatively consistent wind regimes. However, in more complex environments like the Indian Ocean, where wind patterns exhibit significant seasonal and spatial variability due to phenomena such as monsoons, the domain selection for the surrogate data generation method requires careful evaluation.

Another important aspect concerns sea level rise. Although sea level rise consistent with the high emission scenario (RCP8.5) was incorporated in the wave model, its influence on wave simulations was not explicitly analyzed, as it was not the focus of the study. The impact of sea level rise is most pronounced in coastal areas, where even a small increase in water level can significantly amplify the coastal wave impacts, leading to flooding and erosion (van de Wal et al., 2023). Understanding the combined effect of sea level rise and waves is important for evaluating the potential climate change impacts on the coast and remains an important area for future research.

While future projections indicate an increase in mean wave heights over the northern NEA, the regional variability in wave climate needs to be carefully analyzed. This need is reinforced by the contrasting trends observed at locations $M3_L$ and $M4_L$. At $M4_L$, a decline in calm sea states along with an increase in moderate and higher wave heights indicates a transition toward more energetic and active wave conditions. Hs distribution at $M3_L$ reflects a shift in waves where moderate waves become less frequent, while both calm and high waves are becoming more dominant. A potential increase in high wave events at $M4_L$ (located to the NW of Ireland) could be due to its exposure to the poleward-shifting storm tracks. While projected higher waves and stable extreme waves at both locations may reflect increased storm severity or regional response of the wave climate under future conditions.

The seasonal spatial plot shows that autumn experiences the greatest overall reduction in Hs and winter shows an increase in Hs across the NEA domain, the location-specific analysis at $M3_L$ and $M4_L$ further validates this trend. In autumn, $M3_L$ shows a shift towards calmer waves and $M4_L$ exhibits stable conditions across all Hs ranges. Both findings support the broader regional signal of declining wave activity in autumn. In winter, when increased Hs is observed along the west coast of Ireland, both locations show an increase in moderate to very high waves. However, extreme wave events continue to occur at both sites across both seasons, emphasizing that while regional trends are useful, location-specific assessments are essential to capture the full range of wave height behavior.

The significant increase in extreme waves during winter at both $M3_L$ and $M4_L$ highlights the elevated risks associated with winter storms in future scenarios. Conversely, summer months are less influenced by extreme events, making them more suitable for activities like sailing. At $M3_L$, the increase in calm conditions across most seasons, except winter, suggests that spring, summer, and autumn offer suitable windows for marine operations. While at $M4_L$, autumn appears to be the most favorable period as it remains relatively stable across all wave height ranges.

The methodology, together with the findings, demonstrates an efficient and physically realistic means of simulating waves in the NEA. By analyzing the full distributions of wave heights, this study provides detailed insights into spatial and temporal patterns of wave climate, offering a deeper understanding of wave behavior beyond mean values. The findings highlight the critical importance of incorporating both regional and seasonal variability into wave climate assessments, which are essential for developing effective mitigation and adaptation strategies under a changing climate.

8. Conclusion

In this study, we developed a robust wave modeling framework that includes finer resolution models for the NEA and Irish coastal waters. The models driven by high-resolution surrogate winds were able to capture the spatio-temporal variability of the wave climate, which is predominantly wind-driven. The analog method was more efficient in terms of time and computational expenses compared to the common downscaling techniques, which made surrogate data a practical resource for long-term assessments of wave climate. The findings provide a reliable foundation for understanding wave dynamics and supporting coastal management under future climate scenarios.

Conflict of Interest

The authors declare no conflicts of interest relevant to this study.

Availability Statement

The ERA5 wind data on single levels were obtained through the Copernicus Climate Change Service (C3S), available at https://cds.climate.copernicus.eu/datasets/reanalysis-era5-single-levels (C3S, 2018; Hersbach et al., 2023). Daily MPI-ESM wind and Sea ice concentration was accessed via Levante and is publicly available through the ESGF archive https://esgf-data.dkrz.de/search/cmip6-dkrz/ (Eyring et al., 2016). Sea level data were sourced from UKCP18 http://catalogue.ceda.ac.uk/uuid/5fcae68057ea43259d0a4530d34e4ba5 (Met Office Hadley Centre, 2018) and IPCC AR6 sea-level projections (Garner et al., 2021). The wave models used, SWAN which can be downloaded from http://swanmodel.sourceforge.net/ (SWAN Team, 2023) and WAM, available via https://github.com/mywave/WAM (ECMWF, 2019b), are open-source models. Bathymetric data, combining GEBCO and INFORMAR, were provided by the Marine Institute. GEBCO data is publicly available through GEBCO Bathymetric Compilation Group (2023), and INFORMAR data can be accessed via https://www.infomar.ie/data. In situ wave data for model validation were also provided by the Marine Institute and are publicly available via the ERDDAP data server (https://erddap.marine.ie/erddap/index.html). Plots presented in this study were generated using Jupyter Notebooks running on JupyterHub, hosted on the Levante HPC system at the German Climate Computing Center (DKRZ).

Acknowledgments

The study is conducted as part of PhD work funded by the Marine Institute, Galway, Ireland under the project "Decadal Wave Prediction of Irish coast" *(MI/CS/20/111)*. AD received funding from the Danish state through the National Centre for Climate Research (NCKF). This work used resources of the Deutsches Klimarechen-zentrum (DKRZ) granted by its Scientific Steering Committee (WLA) under project ID uo1075. We thank DKRZ Helpdesk for their technical support. We, also, acknowledge Dr. Mikhail Dobrynin, Dr. Sebastian Brune and Kieran Lyons, for their insightful discussions and valuable input, which greatly contributed to the progress of this work.

References

Alizadeh, M. J., Kavianpour, M. R., Kamranzad, B., & Etemad-Shahidi, A. (2020). A distributed wind downscaling technique for wave climate modeling under future scenarios. *Ocean Modelling*, *145*, 101513. https://doi.org/10.1016/j.ocemod.2019.101513

Ana Rute Bento, N. S., & Soares, C. G. (2018). Validation of a wave forecast system for Galway Bay., *11*(2), 112–124. https://doi.org/10.1080/1755876X.2018.1470454

Anton, I., & Nash, S. (2020). Application of the IEC technical specification for assessment of wave energy resource: A case study from the west coast of Ireland. Retrieved from https://sword.mtu.ie/ceri/2020/12/1

Atan, R., Goggins, J., & Nash, S. (2016). Development of a high resolution wave model at AMETS using SWAN. In *Proceedings of the Civil Engineering Research in Ireland (CERI) Conference, Galway, Ireland* (pp. 29–30). https://doi.org/10.1080/1755876X.2016.1275495

Baordo, F., Clementi, E., Iovino, D., & Masina, S. (2020). Intercomparison and assessment of wave models at global scale. Retrieved from https://www.cmcc.it/wp-content/uploads/2020/05/TN0287-oda-05-2020.pdf

Barbariol, F., Pezzutto, P., Davison, S., Bertotti, L., Cavaleri, L., Papa, A., et al. (2022). Wind-wave forecasting in enclosed basins using statistically downscaled global wind forcing. *Frontiers in Marine Science*, *9*, 1002786. https://doi.org/10.3389/fmars.2022.1002786

Bauer, E., & Weisse, R. (2000). Determination of high-frequency wind variability from observations and application to north Atlantic wave modeling. *Journal of Geophysical Research*, *105*(C11), 26179–26190. https://doi.org/10.1029/1999JC000066

Bento, A., Gonçalves, M., Campos, R., & Guedes Soares, C. (2016). Comparison between two forecast systems implemented with WAM and WaveWatch 3 for the North Atlantic (p. V003T02A035). https://doi.org/10.1115/OMAE2016-54464

Bento, A. R., Martinho, P., Campos, R., & Guedes Soares, C. (2011). Modelling wave energy resources in the Irish west coast. In *International Conference on Offshore Mechanics and Arctic Engineering* (Vol. 44373, pp. 945–953). https://doi.org/10.1115/OMAE2011-50346

Bertin, X., Prouteau, E., & Letetrel, C. (2013). A significant increase in wave height in the North Atlantic Ocean over the 20th century. *Global and Planetary Change*, *106*, 77–83. https://doi.org/10.1016/j.gloplacha.2013.03.009

Bingölbali, B., Akpınar, A., Jafali, H., & Vledder, G. P. V. (2019). Downscaling of wave climate in the western Black Sea. *Ocean Engineering*, *172*, 31–45. https://doi.org/10.1016/j.oceaneng.2018.11.042

Bitner-Gregersen, E. M., Waseda, T., Parunov, J., Yim, S., Hirdaris, S., Ma, N., & Soares, C. G. (2022). Uncertainties in long-term wave modelling. *Marine Structures*, *84*, 103217. https://doi.org/10.1016/j.marstruc.2022.103217

Bocquet, M. (2023). Surrogate modeling for the climate sciences dynamics with machine learning and data assimilation. *Frontiers in Applied Mathematics and Statistics*, *9*, 1133226. https://doi.org/10.3389/fams.2023.1133226

Booij, N., Ris, R. C., & Holthuijsen, L. H. (1999). A third-generation wave model for coastal regions: 1. Model description and validation. *Journal of Geophysical Research*, *104*(C4), 7649–7666. https://doi.org/10.1029/98JC02622

Brown, J. M., Souza, A. J., & Wolf, J. (2010). An 11-year validation of wave-surge modelling in the Irish Sea, using a nested POLCOMS–WAM modelling system. *Ocean Modelling*, *33*(1), 118–128. https://doi.org/10.1016/j.ocemod.2009.12.006

C3S. (2018). ERA5 hourly data on single levels from 1940 to present [Dataset]. *Copernicus Climate Change Service (C3S) Climate Data Store (CDS)*. https://doi.org/10.24381/CDS.ADBB2D47

Calvino, C., Dabrowski, T., & Dias, F. (2022). Current interaction in large-scale wave models with an application to Ireland. *Continental Shelf Research*, *245*, 104798. https://doi.org/10.1016/j.csr.2022.104798

Cavaleri, L., Fox-Kemper, B., & Hemer, M. (2012). Wind waves in the coupled climate system. *Bulletin of the American Meteorological Society*, *93*(11), 1651–1661. https://doi.org/10.1175/BAMS-D-11-00170.1

Chen, J., Kang, S., Du, W., Guo, J., Xu, M., Zhang, Y., et al. (2021). Perspectives on future sea ice and navigability in the Arctic. *The Cryosphere*, *15*(12), 5473–5482. https://doi.org/10.5194/tc-15-5473-2021

Dauner, A. L. L., Schenk, F., Power, K. E., & Heikkilä, M. (2024). Sea-ice variations and trends during the common era in the Atlantic sector of the Arctic Ocean. *The Cryosphere*, *18*(3), 1399–1418. https://doi.org/10.5194/tc-18-1399-2024

De Bruin, K. C., & Kyei, C. K. (2024). *Climate change adaptation options and their associated costs and benefits in Ireland* (Tech. Rep.). ESRI Working Paper.

Dodet, G., Bertin, X., & Taborda, R. (2010). Wave climate variability in the north-east Atlantic Ocean over the last six decades. *Ocean Modelling*, *31*(3), 120–131. https://doi.org/10.1016/j.ocemod.2009.10.010

Dodet, G., Melet, A., Ardhuin, F., Bertin, X., Idier, D., & Almar, R. (2019). The contribution of wind-generated waves to coastal sea-level changes. *Surveys in Geophysics*, *40*(6), 1563–1601. https://doi.org/10.1007/s10712-019-09557-5

Düsterhus, A., & Brune, S. (2024). Decadal predictability of seasonal temperature distributions. *Geophysical Research Letters*, *51*(11), e2023GL107838. https://doi.org/10.1029/2023GL107838

Düsterhus, A., & Hense, A. (2012). Advanced information criterion for environmental data quality assurance. *Advances in Science and Research*, *8*(1), 99–104. https://doi.org/10.5194/asr-8-99-2012

ECMWF. (2016). *IFS documentation CY41r2*. ECMWF Reading, UK.

ECMWF. (2019a). *ERA5 reanalysis (0.25 degree latitude-longitude grid)*. Research Data Archive at the National Center for Atmospheric Research, Computational and Information Systems Laboratory. Retrieved from https://rda.ucar.edu/datasets/dsd633000/

ECMWF. (2019b). IFS documentation CY46R1 - Part VII: ECMWF wave model [Software]. *ECMWF*. https://doi.org/10.21957/21G1HOIUO

Eyring, V., Bony, S., Meehl, G. A., Senior, C. A., Stevens, B., Stouffer, R. J., & Taylor, K. E. (2016). Overview of the coupled model intercomparison project phase 6 (CMIP6) experimental design and organization [Dataset]. *Geoscientific Model Development*, *9*(5), 1937–1958. https://doi.org/10.5194/gmd-9-1937-2016

Farrok, O., Farah, M. M., & Islam, M. R. (2024). Introduction to the principles of wave energy conversion. In O. Farrok & M. R. Islam (Eds.), *Oceanic wave energy conversion: Advancement of electrical generators* (pp. 1–15). Springer Nature. https://doi.org/10.1007/978-981-99-9814-2_1

Fedele, F., Herterich, J., Tayfun, A., & Dias, F. (2019). Large nearshore storm waves off the Irish Coast. *Scientific Reports*, *9*(1), 15406. https://doi.org/10.1038/s41598-019-51706-8

Fox-Kemper, B., Hewitt, H. T., Xiao, C., Aðalgeirsdóttir, G., Drijfhout, S. S., Edwards, T. L., et al. (2021). Ocean, cryosphere and sea level change. In V. Masson-Delmotte, et al. (Eds.), *Climate Change 2021: The Physical Science Basis. Contribution of Working Group I to the Sixth Assessment Report of the Intergovernmental Panel on Climate Change* (pp. 1211–1362). Cambridge University Press. https://doi.org/10.1017/9781009157896.011

Gallagher, S., Gleeson, E., Tiron, R., McGrath, R., & Dias, F. (2016a). Twenty-first century wave climate projections for Ireland and surface winds in the north Atlantic Ocean. *Advances in Science and Research*, *13*, 75–80. https://doi.org/10.5194/asr-13-75-2016

Gallagher, S., Gleeson, E., Tiron, R., McGrath, R., & Dias, F. (2016b). Wave climate projections for Ireland for the end of the 21st century including analysis of EC-Earth winds over the North Atlantic Ocean. *International Journal of Climatology*, *36*(14), 4592–4607. https://doi.org/10.1002/joc.4656

Gallagher, S., Tiron, R., & Dias, F. (2014). A long-term nearshore wave hindcast for Ireland: Atlantic and Irish Sea coasts (1979–2012). *Ocean Dynamics*, *64*(8), 1163–1180. https://doi.org/10.1007/s10236-014-0728-3

Gallagher, S., Tiron, R., Whelan, E., Gleeson, E., Dias, F., & McGrath, R. (2016). The nearshore wind and wave energy potential of Ireland: A high resolution assessment of availability and accessibility. *Renewable Energy*, *88*, 494–516. https://doi.org/10.1016/j.renene.2015.11.010

Garcia-Pereira, F., González-Rouco, J. F., & Johann, J. (2023). MPI-ESM1.2-LR p2k+ with a deep version of JSBACH (MPI-ESM p2k+d). https://doi.org/10.5281/ZENODO.10364950

Garner, G. G., Hermans, T., Kopp, R. E., Slangen, A. B. A., Edwards, T. L., Levermann, A., et al. (2021). IPCC AR6 sea level projections [Dataset]. *Zenodo*. https://doi.org/10.5281/zenodo.5914709

Gaughan, E., & Fitzgerald, B. (2020). An assessment of the potential for co-located offshore wind and wave farms in Ireland. *Energy*, *200*, 117526. https://doi.org/10.1016/j.energy.2020.117526

GEBCO Bathymetric Compilation Group. (2023). The GEBCO_2023 grid—A continuous terrain model of the global oceans and land [Dataset]. *NERC EDS British Oceanographic Data Centre NOC*. https://doi.org/10.5285/f98b053b-0cbc-6c23-e053-6c86abc0af7b

Gentile, E. S., Zhao, M., & Hodges, K. (2023). Poleward intensification of midlatitude extreme winds under warmer climate. *npj Climate and Atmospheric Science*, *6*(1), 219. https://doi.org/10.1038/s41612-023-00540-x

Getter, D., Bessac, J., Rudi, J., & Feng, Y. (2024). Statistical treatment of convolutional neural network superresolution of inland surface wind for subgrid-scale variability quantification. *Artificial Intelligence for the Earth Systems*, *3*(1), e230009. https://doi.org/10.1175/AIES-D-23-0009.1

Gleeson, E., Clancy, C., Zubiate, L., Janjić, J., Gallagher, S., & Dias, F. (2019). Teleconnections and extreme ocean states in the northeast Atlantic Ocean. *Advances in Science and Research*, *16*, 11–29. https://doi.org/10.5194/asr-16-11-2019

Guisado-Pintado, E. (2020). Shallow water wave modelling in the nearshore (SWAN). *Sandy Beach Morphodynamics*, 391–419. (Publication Title: Sandy Beach Morphodynamics). https://doi.org/10.1016/B978-0-08-102927-5.00017-5

Günther, H., Hasselmann, S., & Janssen, P. A. (1992). *The WAM model cycle 4 (revised version)*. Deutsches KlimaRechenZentrum.

Hersbach, H., Bell, B., Berrisford, P., Biavati, G., Horányi, A., Muñoz Sabater, J., et al. (2023). ERA5 hourly data on single levels from 1940 to present [Dataset]. *Copernicus Climate Change Service (C3S) Climate Data Store (CDS)*. https://doi.org/10.24381/cds.adbb2d47

Ilyina, T., Six, K. D., Segschneider, J., Maier-Reimer, E., Li, H., & Nunez-Riboni, I. (2013). Global ocean biogeochemistry model HAMOCC: Model architecture and performance as component of the MPI-Earth system model in different CMIP5 experimental realizations. *Journal of Advances in Modeling Earth Systems*, *5*(2), 287–315. https://doi.org/10.1029/2012MS000178

Ivanov, V. V., & Repina, I. A. (2018). The effect of seasonal variability of Atlantic water on the Arctic Sea ice cover. *Izvestiya - Atmospheric and Oceanic Physics*, *54*(1), 65–72. https://doi.org/10.1134/S0001433818010061

Janssen, P., & Bidlot, J.-R. (2003). Part VII: ECMWF wave-model documentation. In *IFS documentation cycle CY23R4* (Vol. 46). ECMWF.

Jungclaus, J. H., Fischer, N., Haak, H., Lohmann, K., Marotzke, J., Matei, D., et al. (2013). Characteristics of the ocean simulations in the Max Planck Institute Ocean Model (MPIOM) the ocean component of the MPI-Earth system model. *Journal of Advances in Modeling Earth Systems*, *5*(2), 422–446. https://doi.org/10.1002/jame.20023

Kandrot, S., Farrell, E., & Devoy, R. (2016). The morphological response of foredunes at a breached barrier system to winter 2013/2014 storms on the southwest coast of Ireland. *Earth Surface Processes and Landforms*, *41*(14), 2123–2136. https://doi.org/10.1002/esp.4003

Kopp, R. E., Garner, G. G., Hermans, T. H. J., Jha, S., Kumar, P., Reedy, A., et al. (2023). The framework for assessing changes to sea-level (FACTS) v1.0: A platform for characterizing parametric and structural uncertainty in future global, relative, and extreme sea-level change. *Geoscientific Model Development*, *16*(24), 7461–7489. https://doi.org/10.5194/gmd-16-7461-2023

Lalbeharry, R., & Ritchie, H. (2009). Wave simulation using SWAN in nested and unnested mode applications.

Lemos, G., Semedo, A., Kumar, R., Dobrynin, M., Akpinar, A., Kamranzad, B., et al. (2023). Performance evaluation of a global CMIP6 single forcing, multi wave model ensemble of wave climate simulations. *Ocean Modelling*, *184*, 102237. https://doi.org/10.1016/j.ocemod.2023.102237

Loureiro, C., & Cooper, A. (2019). Temporal variability in winter wave conditions and storminess in the northwest of Ireland. *Irish Geography*, *51*(2), 155–170. https://doi.org/10.55650/igj.2018.1369

Lowe, J. A., Bernie, D., Bett, P., Bricheno, L., Brown, S., Calvert, D., et al. (2018). UKCP18 science overview report (pp. 1–73).

Luzia, G., Hahmann, A., & Koivisto, M. (2022). Evaluating the mesoscale spatio-temporal variability in simulated wind speed time series over northern Europe. *Wind Energy Science*, *7*(6), 2255–2270. https://doi.org/10.5194/wes-7-2255-2022

Madden, N., Olbert, I., & Shchepetkin, A. (2025). *Tidal research reveals power of storm Éowyn and unfathomable near-miss*. University of Galway News Article. Retrieved from https://www.universityofgalway.ie/about-us/news-and-events/news-archive/2025/april/tidal-research-reveals-power-of-storm-eowyn-and-unfathomable-near-miss--.html

Marine Institute. (2022). Irish marine data buoy observation network. Retrieved from https://www.marine.ie/site-area/infrastructure-facilities/marine-research-infrastructures/irish-marine-data-buoy

Markina, M., Gavrikov, A., Gulev, S., & Barnier, B. (2018). Developing configuration of WRF model for long-term high-resolution wind wave hindcast over the North Atlantic with WAVEWATCH III. *Ocean Dynamics*, *68*(11), 1593–1604. https://doi.org/10.1007/s10236-018-1215-z

Markina, M., Studholme, J. H. P., & Gulev, S. K. (2019). Ocean wind wave climate responses to wintertime North Atlantic atmospheric transient eddies and low-frequency flow. *Journal of Climate*, *32*(17), 5619–5638. https://doi.org/10.1175/JCLI-D-18-0595.1

Melet, A., Meyssignac, B., Almar, R., & Le Cozannet, G. (2018). Under-estimated wave contribution to coastal sea-level rise. *Nature Climate Change*, *8*(3), 234–239. https://doi.org/10.1038/s41558-018-0088-y

Met Office Hadley Centre. (2018). UKCP18 simulations of sea surface elevation for UK waters [Dataset]. *Centre for Environmental Data Analysis*. Retrieved from http://catalogue.ceda.ac.uk/uuid/5fcae68057ea43259d0a4530d34e4ba5

Morales-Márquez, V., Orfila, A., Simarro, G., & Marcos, M. (2020). Extreme waves and climatic patterns of variability in the eastern North Atlantic and Mediterranean basins. *Ocean Science*, *16*(6), 1385–1398. https://doi.org/10.5194/os-16-1385-2020

Neill, S. P. (2024). Wave resource characterization and co-location with offshore wind in the Irish Sea. *Renewable Energy*, *222*, 119902. https://doi.org/10.1016/j.renene.2023.119902

Noël, T., Loukos, H., Defrance, D., Vrac, M., & Levavasseur, G. (2021). A high-resolution downscaled CMIP5 projections dataset of essential surface climate variables over the globe coherent with the ERA5 reanalysis for climate change impact assessments. *Data in Brief*, *35*, 106900. https://doi.org/10.1016/j.dib.2021.106900

O'Brien, L., Dudley, J. M., & Dias, F. (2013). Extreme wave events in Ireland: 14 680 BP–2012. *Natural Hazards and Earth System Sciences*, *13*(3), 625–648. https://doi.org/10.5194/nhess-13-625-2013

Olonscheck, D., Suarez-Gutierrez, L., Milinski, S., Beobide-Arsuaga, G., Baehr, J., Fröb, F., et al. (2023). The New Max Planck Institute grand ensemble with CMIP6 forcing and high-frequency model output. *Journal of Advances in Modeling Earth Systems*, *15*(10), e2023MS003790. https://doi.org/10.1029/2023MS003790

Palermo, R. V., Perron, J. T., Soderblom, J. M., Birch, S. P. D., Hayes, A. G., & Ashton, A. D. (2024). NEWTS1.0: Numerical model of coastal erosion by waves and transgressive scarps. *Geoscientific Model Development*, *17*(8), 3433–3445. https://doi.org/10.5194/gmd-17-3433-2024

Paranunzio, R., Guerrini, M., Dwyer, E., Alexander, P. J., & O'Dwyer, B. (2022). Assessing coastal flood risk in a changing climate for Dublin, Ireland. *Journal of Marine Science and Engineering*, *10*(11), 1715. https://doi.org/10.3390/jmse10111715

Pilar, P., Soares, C. G., & Carretero, J. C. (2008). 44-year wave hindcast for the North East Atlantic European coast. *Coastal Engineering*, *55*(11), 861–871. https://doi.org/10.1016/j.coastaleng.2008.02.027

Pinto, J. G., Bellenbaum, N., Karremann, M. K., & Della-Marta, P. M. (2013). Serial clustering of extratropical cyclones over the North Atlantic and Europe under recent and future climate conditions. *Journal of Geophysical Research: Atmospheres*, *118*(22), 12476–12485. https://doi.org/10.1002/2013JD020564

Reduan Atan, S. N., & Goggins, J. (2017). Development of a nested local scale wave model for a 1/4 scale wave energy test site using, SWAN. *Journal of Operational Oceanography*, *10*(1), 59–78. https://doi.org/10.1080/1755876X.2016.1275495

Reick, C. H., Raddatz, T., Brovkin, V., & Gayler, V. (2013). Representation of natural and anthropogenic land cover change in MPI-ESM. *Journal of Advances in Modeling Earth Systems*, *5*(3), 459–482. https://doi.org/10.1002/jame.20022

Rezvov, V., Krinitskiy, M., & Gulev, S. (2022). Approximation of high-resolution surface wind speed in the North Atlantic using discriminative and generative neural models based on RAS-NAAD 40-year hindcast (p. 23). https://doi.org/10.22323/1.429.0023

Rozoff, C. M., & Alessandrini, S. (2022). A comparison between analog ensemble and convolutional neural network empirical-statistical downscaling techniques for reconstructing high-resolution near-surface wind. *Energies*, *15*(5), 1718. https://doi.org/10.3390/en15051718

Rusu, L., Pilar, P., & Guedes Soares, C. (2008). Hindcast of the wave conditions along the West Iberian coast. *Coastal Engineering*, *55*(11), 906–919. https://doi.org/10.1016/j.coastaleng.2008.02.029

Scott, T., Wiggins, M., Masselink, G., Castelle, B., Dodet, G., & Saulter, A. (2019). Atmospheric climate control of directional waves in the United Kingdom and Ireland. In *Coastal Sediments 2019* (pp. 708–721). https://doi.org/10.1142/9789811204487_0063

Senter, J., & Lupo, A. (2024). A Euclidean distance diagnostic of North Atlantic basin activity. https://doi.org/10.21203/rs.3.rs-3869007/v1

Sheehan, Kevin and INFOMAR Survey Team. (2021). CV20_02 INFOMAR survey report. Retrieved from http://hdl.handle.net/10793/1733

Stevens, B., Giorgetta, M., Esch, M., Mauritsen, T., Crueger, T., Rast, S., et al. (2013). Atmospheric component of the MPI-m Earth system model: ECHAM6. *Journal of Advances in Modeling Earth Systems*, *5*(2), 146–172. https://doi.org/10.1002/jame.20015

Swain, J., Umesh, P., & Balchand, A. (2019). WAM and WAVEWATCH-III intercomparison studies in the north Indian Ocean using OCEANSAT-2 scatterometer winds. *Journal of Ocean and Climate: Science, Technology and Impacts*, *9*, 2516019219866569. https://doi.org/10.1177/2516019219866569

SWAN Team. (2023). Swan—Scientific and technical documentation (Version 41.45) [Software]. Retrieved from http://www.swan.tudelft.nl

Tiron, R., Gallagher, S., Gleeson, E., Dias, F., & McGrath, R. (2013). The future wave climate of Ireland: From averages to extremes. In *Procedia IUTAM* (Vol. 17, pp. 40–46). https://doi.org/10.1016/j.piutam.2015.06.007

Tolman, H. L. (1989). The numerical model WAVEWATCH: A third generation model for hindcasting of wind waves on tides in shelf seas.

Towe, R., Eastoe, E., Tawn, J., & Jonathan, P. (2017). Statistical downscaling for future extreme wave heights in the North Sea. *Annals of Applied Statistics*, *11*(4), 2375–2403. https://doi.org/10.1214/17-AOAS1084

Tuomi, L., Kanarik, H., Björkqvist, J.-V., Marjamaa, R., Vainio, J., Hordoir, R., et al. (2019). Impact of ice data quality and treatment on wave hindcast statistics in seasonally ice-covered seas. *Frontiers in Earth Science*, *7*, 166. https://doi.org/10.3389/feart.2019.00166

van de Wal, R. S., Melet, A., Bellafiore, D., Vousdoukas, M., Camus, P., Ferrarin, C., et al. (2023). Sea level rise in Europe: Impacts and consequences. *State of the Planet Discussions*, *2023*, 1–65. https://doi.org/10.5194/sp-3-slre1-5-2024

Vousdoukas, M. I., Mentaschi, L., Voukouvalas, E., Verlaan, M., & Feyen, L. (2017). Extreme sea levels on the rise along Europe's coasts. *Earth's Future*, *5*(3), 304–323. https://doi.org/10.1002/2016EF000505

WAMdi Group. (1988). The WAM model—A third generation ocean wave prediction model. *Journal of physical oceanography*, *18*(12), 1775–1810. https://doi.org/10.1175/1520-0485(1988)018⟨1775:TWMTGO⟩2.0.CO;2

Zed, A. A. A., Kansoh, R. M., Iskander, M. M., & Elkholy, M. (2022). Wind and wave climate southeastern of the Mediterranean Sea based on a high-resolution SWAN model. *Dynamics of Atmospheres and Oceans*, *99*, 101311. https://doi.org/10.1016/j.dynatmoce.2022.101311

Zhang, D., Tang, N., Dong, W., & Zhao, L. (2024). Machine learning-based financial big data analysis and forecasting: From preprocessing to deep learning models. *Applied and Computational Engineering*, *116*(1), 143–149. https://doi.org/10.54254/2755-2721/116/20251731